2013

Electrical and Thermal Response of Carbon Nanoture Composites Under Quasi-Static and Dynamic Loading

Christopher D. O'Connell
University of Rhode Island, chrsr34@hotmail.com

ELECTRICAL AND THERMAL RESPONSE OF CARBON NANOTUBE COMPOSITES UNDER QUASI-STATIC AND DYNAMIC LOADING

BY

CHRISTOPHER D. O'CONNELL

A THESIS SUBMITTED IN PARTIAL FULFILLMENT OF THE REQUIREMENTS FOR THE DEGREE OF

MASTER OF SCIENCE

IN

MECHANICAL, INDUSTRIAL, AND SYSTEMS ENGINEERING

UNIVERSITY OF RHODE ISLAND

2013

MASTER OF SCIENCE THESIS

OF

CHRISTOPHER D. O'CONNELL

APPROVED:

Thesis Committee:

Major Professor Arun Shukla

Sze Yang

Donna Meyer

Nasser H. Zawia

DEAN OF THE GRADUATE SCHOOL

UNIVERSITY OF RHODE ISLAND
2013

ABSTRACT

Carbon nanotube (CNT) composites have attracted much interest due to their possible technical applications as conductive polymers and sensory materials. This study will consist of two major objectives: 1.) to investigate the thermal conductivity and thermal response of multi-wall carbon nanotube (MWCNT) composites under quasi-static loading, and 2.) to investigate the electrical response of carboxyl-terminated butadiene (CTBN) rubber-reinforced MWCNT/Epoxy composites under quasi-static and dynamic loading. Similar studies have shown that the electrical conductivity of CNT/Epoxy composites dramatically increases with compressive strains up to 15%. Part 1 seeks to find out if thermal conductivity shows a similar response to electrical conductivity under an applied load. Part 2 seeks to investigate how the addition of rubber affects the mechanical and electrical response of the composite subjected to quasi-static and dynamic loading. By knowing how thermal and electrical properties change under a given applied strain, we attempt to broaden the breadth of understanding of CNT/epoxy composites and inquire the microscopic interactions occurring between the two.

Electrical experiments sought to investigate the electrical response of rubber-reinforced carbon nanotube epoxy composites under quasi-static and dynamic loading. Specimens were fabricated with CTBN rubber content of 10 parts per hundredth resin (phr), 20 phr, 30 phr and 0 phr for a basis comparison. Both quasi-static and dynamic mechanical response showed a consistent decrease in peak stress and Young's modulus with increasing rubber content. Trends in the electrical response between each case were clearly observed with peak resistance changes ranging from 58% to

73% and with each peak occurring at a higher value with increasing rubber content, with the exception of the rubber-free specimens. It was concluded that among the rubber-embedded specimens, the addition of rubber helped to delay micro-cracking and degradation and thus prolong the electrical response of the specimen to higher strains.

Thermal experiments were first established by designing and fabricating an apparatus to determine the thermal conductivity of an unknown material. The principle of the apparatus is a steady-state one-dimensional comparative method where reference materials of known thermal conductivity are used to determine the system heat flux and in turn, the thermal conductivity of a given specimen. A thermal percolation study was conducted in order to determine a possible threshold of thermal transport of the material. The recorded values of thermal conductivity from 0 – 0.2 wt% showed no such threshold with all specimens of different CNT loadings yielding similar values of thermal conductivity. The apparatus containing the CNT/epoxy specimen was then quasi-statically compressed to observe how the thermal conductivity changes with strains up to 20%. While a small decrease in thermal conductivity was observed under strain, it can mostly be attributed to material degradation and bulging.

ACKNOWLEDGMENTS

I would like to firstly thank Dr. Arun Shukla for his continuous guidance and creating a truly enjoyable graduate experience. His charisma, positive suggestiveness, and unique approach to solving problems created a challenging and fulfilling work environment that I enjoyed to enter every day.

I would also like to thank Dr. Vijaya Chalivendra, Dr. Sze Yang, Dr. Keunhan Park, and Dr. Donna Meyer for their continuous support in my research and graduate studies. I learned so much from each one of them and will continue to look to them as mentors as I begin my career.

I owe so much to those in the Dynamic Photomechanics Laboratory. From troubleshooting to experimental setup to result interpretation; there was no limit to the amount of achievable success working as a team. Notably, Nick Heeder, Prathamesh Parrikar, Payam Fahr, Frank LiVolsi, Sachin Gupta, Sandeep Abotula, Emad Maki, and Chris Schillings . As we all move on to our future successes, I know that I always have a second family to rely upon to solve any problem.

I am tremendously gracious to the National Science Foundation (NSF) for their support through the CMMI 0856133 grant directed by Dr. Glaucio H. Paulino.

Lastly, I would like to thank my father, David, mother, Manuela, and brother, Brian, for their boundless support in all the things that I do. They have undeniably encouraged all choices that I have made and all the paths I have taken. I really would not be where I am without them.

TABLE OF CONTENTS

LIST OF TABLES

LIST OF FIGURES

FIGURE PAGE

CHAPTER 1

INTRODUCTION

Carbon nanotubes have raised a considerable amount of interest in recent years due to their exceptionally unique mechanical, electrical, and thermal properties. These quasi-one-dimensional molecules consist of a covalently bonded hexagonal lattice of carbon atoms rolled into a tubule configuration. This roll angle, or chirality, determines the properties of the nanotube, which are generally lumped as being a conductor or a semiconductor. Multi-wall carbon nanotubes (MWCNT) are formed when more than one sheet circumscribes the tube axis. Because MWCNT will on average have both conductor and semiconductor layers embedded, they are usually defined as a zero-gap metal and highly conductive.

The extraordinary properties that CNT display make it a perfect candidate as a filler material in composite structures. When uniformly dispersed within a polymer matrix, the nanotubes form an electrical sensory network which can be used to detect important information about material damage and degradation under mechanical loading. In application, this composite could be used to monitor the mechanical state of a structure under loading by inquiring its electrical resistance. The pursuit to exploit these unique characteristics has engendered some novel ideas and applications across a large spectrum of industries.

This study will take on a two-part investigation in order to further understand the fundamental properties and responses of this unique composite. Part one seeks to understand the electrical response of carboxyl-terminated butadiene (CTBN) rubber

reinforced CNT/epoxy composites under compressive quasi-static loading and dynamic loading via split Hopkinson pressure bar (SHPB). The influence of four different weight fractions of CTBN resin (0, 10, 20, and 30 parts per hundredth resin, or phr) with a constant CNT loading of 0.2 wt% on the electrical response under said loadings was studied. A four-point and semi-four-point probe method was used to capture the electrical response in quasi-static and dynamic experiments, respectively. High speed photography was used in dynamic experiments to provide a better insight to the mechanisms of damage and a direct correlation to electrical response.

Part two of this study seeks to investigate and confirm how the thermal conductivity changes in epoxy with different loadings of CNT, and also how the thermal conductivity changes under quasi-static loading. An apparatus to probe the thermal conductivity was developed using a comparative method in which the heat flux is determined by reference materials with known thermal conductivity. This is a one-dimensional (1-D) steady-state heat flow method and therefore the 1-D heat equation was used to calculate the thermal conductivity. This apparatus was also designed to withstand mechanical loading so that the thermal conductivity of the composite could be determined under loading.

This study will attempt to fill some of the gaps that still exist in understanding this interesting sensory composite. The introduction of a second filler material such as CTBN rubber opens a new door to modifying and tailoring the composite to specific and desirable properties and responses. The thermal response under loading has yet to be investigated by other teams and thus these preliminary experiments will provide a starting point for further study.

CHAPTER 2

REVIEW OF LITERATURE

Recently, a large amount of research has been employed to understand the benefits of CNTs as a filler material in a conventional polymer matrix. This review will attempt to itemize the key findings of carbon nanotubes and their implementation into an epoxy matrix.

The discovery of carbon nanotubes came in 1991 when they were synthesized using an arc-discharge evaporation method [Iijima et al, 1991]. The structure of a carbon nanotube comprises of coaxial tubes of graphene sheets, ranging in number to form single and multi-wall nanotube structures. The carbon atoms of the nanotube assume a hexagonal lattice with different properties depending on the roll angle, or chirality, of the nanotube. This carbon-crystalline structure leads to a number of unique findings. Theoretical and experimental results have shown that CNTs can have an elastic modulus as high as 1 TPa (the elastic modulus of diamond is 1.2 TPa) with a strength several magnitudes higher than that of steel at a fraction of the weight [Thostenson et al, 2001]. CNT have also shown exceptional thermal properties exceeding that of diamond with reported values of thermal conductivity between 1750 – 6000 W/mK [Hone et al, 1999, Berber et al, 2000, Fujii et al, 2005]. Electrically, CNT have been found to have a current-carrying capacity 1000 times higher than that of copper [Collins et al, 2000]. These excellent properties inspire interest in using CNTs as fillers in various types of composite materials.

Using CNT as a filler material in a polymer matrix to form a "nanocomposite" has been of increasing interest in order to exploit many of the findings of this nanomaterial. It has been shown that CNTs can be used to significantly enhance mechanical, thermal, and electrical properties of a polymer matrix when introduced as a filler material. Among the range of polymers available today, high strength industrial epoxy serves as a versatile material for aerospace, electronics, and structural industries due to its high strength, light weight, ease of use, and low cost.

In order to exploit the excellent properties of CNTS within a polymer, the nanotubes must be effectively and uniformly dispersed. Because the carbon atoms use all their electrons to form the robust carbon-carbon covelant bonds, weak Van Der Waals forces cause the nanotubes to loosely attach and agglomerate into bundles. This phenomenon necessitates a method to properly disperse the nanotubes within the polymer matrix. A number of methods have been developed to achieve uniform dispersion matrices [Breuer et al, 2004, Xie et al, 2005, Moniruzzaman et al, 2006, Fiedler et al, 2006, Gibson et al, 2007, Bal et al, 2007). Functionalized CNTs coupled with mixing techniques such as ultra–sonication and shear mixing have been shown to achieve adequate dispersion in polymer composites [Bauhofer et al, 2009]. The high aspect ratio and high conductivity make it possible to have very a low percolation threshold falling between 0.1-0.2 wt% CNT [Sandler et al, 2003, Grulan et al, 2004, Kymakis et al, 2006, Du et al, 2004, Hu et al, 2006, Shenogina et al, 2005, Pham et al, 2005, Li et al, 2008, Allaoui et al, 2002].

There has been a significant amount of research done to enhance mechanical properties of CNT-polymer composites. The Young's modulus and the yield strength

have been doubled and quadrupled (in tension) for composites with respectively 1 and 4 wt% nanotubes, compared to pure resin matrix samples [Allaoui et al, 2002]. Coleman et al. (2006) summarized much of the progress to date in the field of mechanical reinforcement of polymers using carbon nanotubes with a focus on the enhancement of Young's modulus, strength, and toughness.

A gross amount of effort has been applied to the investigation of the electrical response of CNT/polymer composites. Alexopoulos et al. (2009) performed various incremental tensile loading-unloading steps as well as three-point bending tests on specimens with CNT fibers in the tensile region. Alexopoulos also performed various tests on CNT-embedded glass fiber reinforced polymers (GRFP) for structural health monitoring of the composite under mechanical load. Results showed that the electrical response provided by the CNT fiber network provided reliable and repeatable information for sensing and damage monitoring of non-conductive composites under compressive and tensile loading. Gao et al. (2009) investigated the sensing of damage evolution in composites using CNT networks and utilizing the electrical response and acoustic emission as damage-sensing techniques. Resistance change and acoustic emission results showed a bi-linear relation in detecting damage in quasi-static and cyclic experiments which can be used to give additional insight in the damage evolution in these composites. Thostenson et al. (2006) performed tensile tests on CNT/epoxy specimens and demonstrated a highly linear relationship between the applied strain and the electrical resistance. This result suggests that uniformly dispersed CNT networks within an epoxy polymer matrix could be utilized as highly sensitive sensors for detecting the evolution of damage in polymer-based composites.

Lim et al. (2011) experimentally investigated the mechanical and electrical response of CNT-based fabric composites using dynamic split Hopkinson pressure bar (SHPB) loading to further demonstrate the effectiveness of a percolation carbon nanotube network being used to sense material damage under loading. An experimental investigation was conducted to study the effect of quasi-static and dynamic compressive loading on the electrical response of MWCN- reinforced epoxy composites [Heeder et al, 2011]. Results showed the electrical resistance to decrease between 40%-60% and then an increase after the initiation of catastrophic damage. Damage sensing of MWCNT/ epoxy composites under quasi-static uniaxial tensile loading was also investigated [Vadlamani et al, 2012]. Two types of particulates were introduced to the composite; (1) aluminum silicate hollow microspheres (cenospheres) and (2) liquid carboxyl-terminated butadiene acrylonitrile (CTBN) rubber. Several stages of damage were mapped by the non-linear U-shaped electrical response and thus exploited the CNT as a sensory network to provide early warning of composite failure.

A large effort has also been invested into the thermal properties of CNT/epoxy composites. A dependence of CNT content on the glass transition temperature, T_g , was observed and showed an increase from approximately 64°C for plain epoxy to 72°C at various CNT loadings [Gojny et al, 2004]. The electrical and thermal conductivities of epoxy composites containing 0.005-0.5 CNT have been studied [Moisala et al, 2005]. They found that MWCNT composites had an electrical percolation threshold of <0.005 wt% whereas the thermal conductivity of the samples increased more modestly with a peak increase of 11% at 0.5 wt% MWCNT loading.

Interestingly, the same study found a decrease in thermal conductivity for SWCNT. Further thermal conductivity enhancement with respect to CNT filler content in epoxy was found was in several studies [Bryning et al, 2005, Song et al, 2005, Gojny et al, 2006]. A thermal percolation threshold study was conducted on rubber toughened epoxy/CNT composites between 0% and 1% and found it to be approximately 0.4 wt%, although absolute thermal conductivity changes were still relatively low at 16% increase [Balakrishnan et al, 2011]. Hone et al. (1998), among others, has demonstrated that the dominant mechanism of thermal conductivity is acoustic phonons, which has broad implications on thermal heat transfer in composites.

CHAPTER 3

METHODOLOGY

Specimen Preparation

Specimen preparation for both electrical and thermal experiments followed similar procedures. The matrix material used in this study was a two-part epoxy consisting of Buehler Epothin Resin (20-8140-032) and Buehler Epothin Hardener (20-8142-016) with a resin-hardener ratio of 2.546:1. MWCNT from Nanolab Inc. with 30±15 Nm diameter and 5-20 μm length served as the filler of the composite. For electrical experiments, Hypro 1300X13 Polymer CTBN rubber was added to the composite in weight loadings of 0, 10, 20, and 30 phr. This rubber assumes a liquid form at room temperature and is specifically designed to be included in thermoset resins. Thermal specimens did not use CTBN rubber.

Specimen fabrication begins with combining 70g of resin with the appropriate weight percentage of CNT and shear mixing at 350 rpm for 30 minutes. Shear mixing was executed using an Ika Werke RW 16 Basic shear mixer equipped with a R1381 3 blade propeller. Due to previous studies on percolation threshold, a CNT loading of 0.2 weight percent was used for all electrical specimens to form the percolation network. CNT weight percentages of the thermal specimens were 0, 0.05, 0.1 and 0.2. CNT tend to bundle and agglomerate due to weak Van der Waal forces, and therefore energy must be input to break apart and disperse them into a uniform network. Ultrasonication is employed to address this issue. The mixture is ultra-sonicated using a Sonics & Materials Inc. VCX750 sonicator for 1 hour at 75% intensity with an

on/off ratio of 4.5/9.0 seconds. Due to the large amount of heat generated from the high frequency vibrations, the mixture is contained in a copper beaker and partially submerged in an ice bath in order to maintain a mixture temperature of 35°C or less. Humidity was maintained below 35% for all fabrication processes. The general scheme of this process can be seen in Figure 1.

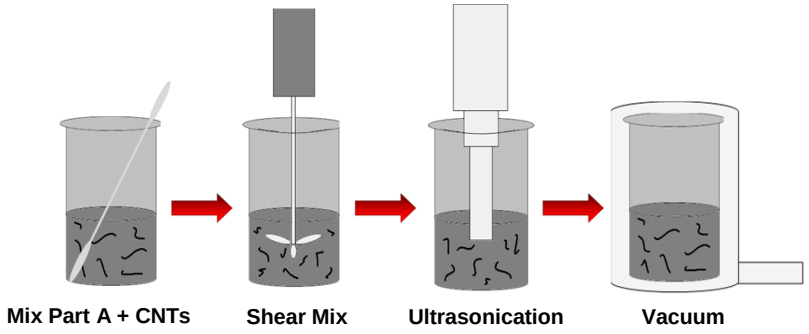

Figure 1 - Schematic of nanocomposite fabrication process

For the electrical specimens, the appropriate loading of rubber is then added, where 10 phr is 7g, 20 phr is 14g, and 30 phr is 21g. It is then shear mixed for 30 minutes at 450 rpm. Because the previous processes introduce a large quantity of air into the mixture, it is then placed in a vacuum chamber for 1 hour or until virtually all air has been removed. Upon removal, 27.3g of hardener is then carefully hand-mixed for 2 minutes and then shear-mixed at 100 rpm for 2 minutes. It is important in the final mixing to avoid introducing air and bubble formation. The mixture is then poured into its appropriate mold and allowed to cure for 48 hours.

Specimen geometries differed for each experiment. Quasi-static electrical specimens were cast and machined into a cylindrical configuration with a length of 0.5” (12.7 mm) and diameter of 0.25” (63.5 mm). SHPB specimens were cylindrical with an equal length and diameter of 0.5” (12.7 mm). Thermal specimens were

molded into a cuboid geometry with a length and width of 1” (25.4 mm) and height of 0.5” (12.7 mm). All molds were fabricated from machinists’ wax. A Buehler release agent (20-8185-002) was applied to the molds before pouring to ensure easy removal after curing.

After fully curing, the specimens were pressed out of their molds and inspected for bubbles and geometrical deficiencies. Electrical specimens are then machined to their desired length using a lathe. Circumferential voltage probe grooves with a depth of 0.005” were then machined into the cylindrical surface of the electrical specimens (Figure 2). The 2 voltage probes are spaced equidistant along the specimen length with spacing of 0.167”. Conductive silver paint is then applied to the top and bottom faces of the specimen as well as the voltage probe grooves. Electrical wire is then wrapped into the voltage probe grooves and a second layer of silver paint is applied to ensure good electrical connection. M-Coat, a polyurethane coating, is finally applied over the voltage probe area to maintain a good connection and prevent wire-debonding during experimental loading.

Thermal specimens were machined to their cuboid geometry using a milling machine. Thermocouple grooves were machined from edge to center onto the top and bottom faces with a depth and width of 0.04” (1.016 mm). It is important to ensure that the thermal specimens maintain a smooth surface to ensure minimal contact resistance. All specimen geometries can be seen in Figure 2.

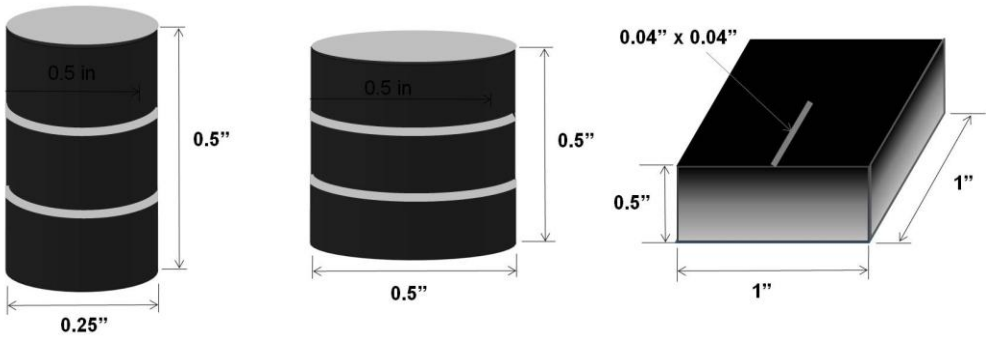

Figure 2 – Quasi-static, dynamic, and thermal specimen geometries

4-Point Probe Method (Quasi-static)

A four-point circumferential probe method was used to record the electrical response of specimens during mechanical loading. This technique was chosen so as to isolate electrical information occurring within the material and independent of contact resistance at the applied interface. This technique also allows the calculation of the initial resistivity of the specimen.

Figure 3 shows a schematic of the probe setup. A constant current is supplied through the specimen via a Keithley 6222 current source. For quasi-static experiments, the specimen is sandwiched between two aluminum plates which are connected to the current source. This allows current to pass uniformly through the volume of the specimen. Both plates are electrically isolated from the top and bottom of the Instron heads by a film of electrical tape. With two equi-distant circumferential probes attached to the inner region of the specimen, each wire was connected to an instrument of voltage detection. Quasi-static experiments run for long periods of time at very slow loading rates and therefore require low-frequency acquisition. Each wire was attached to a Keithley 6514 electrometer (2 in total) and the voltage difference

between the two wires was detected with a Keithley 2000 digital multi-meter. All voltage data was recorded and saved using a LabVIEW program.

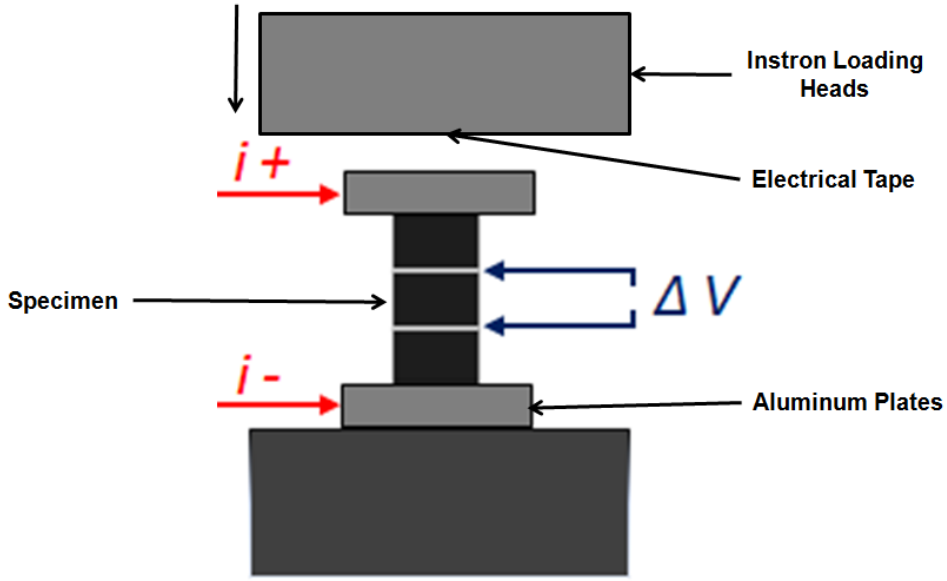

Figure 3 – Quasi-static experimental Setup

Semi 4-Point probe method (Dynamic Experiments)

For dynamic SHPB experiments, due to the high strain rate and relatively short loading event, a slightly different apparatus was used to obtain the electrical response. Current was supplied once again by a Keithly 6222 current source from the incident bar to the transmitted bar of the SHPB apparatus with the specimen sandwiched in between the two. Conductive grease was pasted onto the bar-specimen interfaces to ensure minimal contact resistance and to eliminate shearing and frictional forces at the interfaces. To prevent any current loss or shorting, the bars were insulated from all contact from other metal surfaces and grounds using nylon bushings. This ensures that all the current is passing through the specimen alone. Furthermore, the aluminum striker bar was electrically isolated upon impact with the incident bar with the aid of

one strip of electrical tape and a lead pulse shaper. This prevented any short-circuiting upon impact.

Due to the high-impact nature of the experiment, high frequency acquisition equipment was necessary to capture the electrical response of the specimen. A Tektronix ADA 400A differential amplifier was employed in conjunction with a Tektronix TDS 3014 digital oscilloscope to record the voltage data. Voltage was recorded at points on the incident and transmitted bars, in contrast to the 4-point probe method of quasi-static experiments. This change was made due to inconsistent and anomalous electrical behavior occurring within the specimen with a dedicated 4-point probe configuration. Due to the added contact resistance between the bars and specimen, the absolute value of total resistance is offset to a higher value. This offset remains virtually unchanged within the range of applied strain and was confirmed, to the largest extent possible, by simultaneously comparing both semi 4-point and a dedicated 4-point probe data from the same event.

Quasi-static Experiments

The quasi-static experiments were carried out using an Instron 5585 material testing system and Merlin software. The apparatus consists of a screw-driven head and a mounted base in which to compress the specimen in between. Force and extension data are recorded in real-time as the Instron head loads the specimen. This data was used to calculate the engineering stress and strain of the specimen.

The four point probe method described earlier was used to record the voltage of the center section of the specimens throughout the experiment. Figure 4 shows the

experimental setup with the Instron and four-point probe components. The quasi static experiments were carried out at a compressive extension rate of 0.125 mm/min. Both top and bottom faces of the Instron heads were insulated with electrical tape in order to prevent electrical shorting. The specimen is sandwiched between two aluminum plates in order to pass current through its volume. The plate-specimen sandwich configuration is then placed in between the Instron head and base. An appropriate current is supplied in order to obtain approximately 1 Volt at the inner probes. A preload of approximately 50 N was applied to the specimen to ensure minimal contact resistance between the aluminum plates and the specimen. Quasi-static experiments were initiated simultaneously with the four-point probe system's LabVIEW program so that the stress strain data could be properly correlated with the electrical response of the specimen. The experiments were halted after approximately 20% strain due to excessive bulging and also with the onset of increasing resistance.

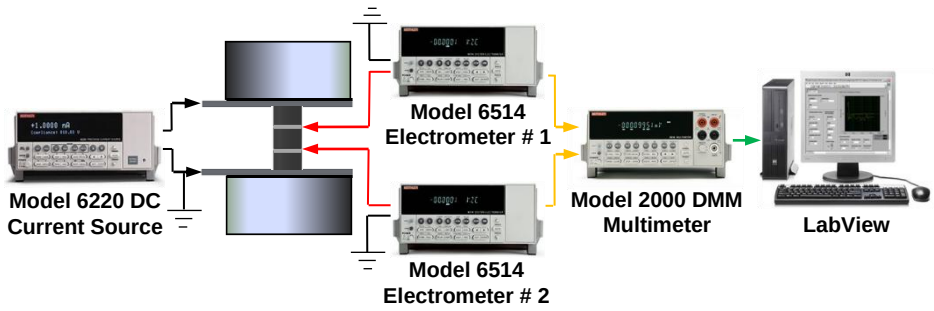

Figure 4 – Quasi-static experimental acquisition scheme

Dynamic Split Hopkinson Pressure Bar Experiments

The split Hopkinson bar technique is a classical experimental technique for dynamic measurements. The advantage of this technique is that it succeeds in

decoupling the inertial effect and the high strain rate effect, which are generally coupled when a material is subjected to a dynamic loading. This makes it possible to determine mechanical properties at high strain rates as high as 10^4.

A schematic of the SHPB apparatus can be seen in figure 5. The main components are the striker, incident, and transmitted bars, all aligned along a single axis. Strain as a function of time is detected by two oppositely-mounted strain gages on the incident and transmitted bars. With the specimen placed between the incident and transmitted bars, the striker is launched by a pressurized gas gun and impacts the incident bar creating an elastic stress wave to propagate along the bar axis. The P-wave propagates through the incident bar as a negative compressive strain. When this strain wave reaches the specimen, it partially reflects in tension and partially is transmitted through the specimen and into the transmitted bar.

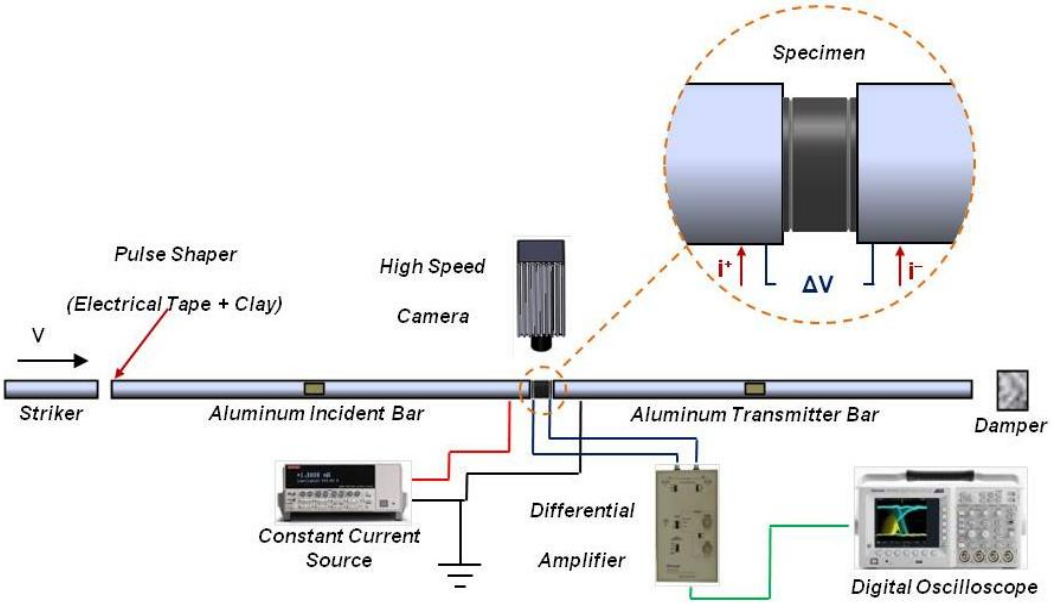

Figure 5 – Split Hopkinson pressure bar apparatus with four-point probe setup

Aluminum incident and transmitted bars were chosen for this experiment as its impedance is desirable for softer materials like epoxy. Incident and transmitted bar diameters were 0.75" (19.05 mm). A conductive lubricant was applied to the bar-specimen interfaces to minimize frictional shearing and effectively pass current with minimal contact resistance. A lead pulse shaper and one piece of electrical tape was used between the striker and incident bar upon impact to obtain the desired strain pulse character to be imparted onto the specimen and also to prevent any electrical shorting from the passage of current through the bars. Strain gage data was obtained using a Wheatstone bridge configuration and a Tektronix 3034D Oscilloscope. Real-time damage was observed using a Photron SA1 high speed camera with a frame rate of 100,000 fps.

Some notable constraints were intrinsic to this experiment. Striker pressures were limited to approximately 125 psi as higher pressures were destroying the insulating electrical tape at the striker-incident bar interface, and also causing rapid damage to the striker and incident bars. A plethora of more robust insulators were tested at higher pressures, yet significantly diminished incident strain pulse shapes. This led to a limit on applied strain and strain rate to be imparted onto the specimens. Given the half-inch length of the specimen, 12-17% strains and strain rates of 700-1000 s^{-1} were obtained at these applied pressures and were sufficient for plastic deformation and sufficient electrical response data. Further experimental optimization could be done by implementing a more robust insulating system and also by reducing the specimen length for increased strain.

Electrical Response Data Analysis

From the constant current input and material voltage data, the resistance was calculated using Ohm's law. The percent change in resistance ΔR within the specimen was then calculated using

$$\Delta R = \left(\frac{R(\varepsilon) - R_o}{R_o}\right) 100 \quad (1)$$

where $R(\varepsilon)$ is the instantaneous resistance as a function of strain and R_o is the initial resistance of the specimen with no applied load. Of particular interest in this study was the peak electrical change at its respective strain value and the electrical response curve shape. Mechanical quantities such as Young's modulus and peak stress were also noted so as to relate the changes in mechanical and electrical response among the varying CTBN rubber loadings.

Thermal Experiments

The objectives of the thermal experiments were to conduct a thermal percolation study and to investigate how thermal conductivity changes with an applied load. In order to determine the thermal conductivity of a material of unknown thermal properties, an apparatus was developed. A comparative one-dimensional (1-D) steady-state conduction method was chosen for the design criteria. In this method, a test specimen of unknown thermal properties is sandwiched between two reference materials of known thermal properties. A temperature gradient is applied across the stack of materials and allowed to reach a steady-state temperature distribution. The stack is insulated circumferentially to minimize heat losses. At equilibrium, the

thermal conductivity of the test specimen is calculated using the temperature gradient and know properties of the reference material.

It is important to first lay the foundation of basic principles of a 1-D steady-state conduction system. The governing equation of such a system can be expressed by the 1-D heat equation of the form

$$q = k(T)\frac{dT}{dx} \tag{2}$$

where q is the heat flux, k(T) is the temperature-dependent thermal conductivity, dT is infinitesimal change in temperature and dx is the infinitesimal change in length. Because of the relatively short range of temperatures used during the experiments, the thermal conductivity was assumed to be a temperature-independent constant. Furthermore, for an ideal 1-D steady-state system, the temperature gradients can be assumed to be linear through each material. These assumptions simplify equation 2 to

$$q = k\frac{T_2 - T_1}{L} \tag{3}$$

where T_2 is the higher temperature, T_1 is the lower temperature, and L is the distant between each point of temperature measurement.

In applying equation 3 to solve for an unknown thermal conductivity k, all other quantities must be determined. The length L is easily determined by the prescribed specimen dimensions. Temperatures T_1 and T_2 were determined by thermocouples at each end of the material. The heat flux q is not easily determined and therefore the use of reference materials is needed. In a 1-D steady state conduction

system, heat flux is constant throughout the entire stack and therefore is the same in the reference materials and test specimen. To specify, the flux through each material is

$$q_{r1} = k_r \frac{T_1 - T_2}{L_r}, q_s = k_s \frac{T_3 - T_4}{L_s}, q_{r2} = k_r \frac{T_5 - T_6}{L_r} \quad (4)$$

where q_{r1} and q_{r2} are the heat flux through each reference material, k_r is the reference thermal conductivity, q_s and k_s are the test specimen heat flux and thermal conductivity, L_r and L_s are the specimen length dimensions in which the gradient is applied, and T_i are the respective temperatures across the specimen. Because heat flux is constant through the stack, $q_{r1} = q_{r2} = q_s$. Using this relation, the unknown thermal conductivity can be determined using the average of the known top and bottom heat flux by

$$k_s = \frac{k_r}{2}\left(\frac{L_s}{T_3 - T_4}\right)\left(\frac{T_1 - T_2}{L_r} + \frac{T_5 - T_6}{L_r}\right) \quad (5)$$

$$= \left(\frac{q_{r1} + q_{r2}}{2}\right)\left(\frac{L_s}{T_3 - T_4}\right).$$

This is a highly idealized situation as it assumes no circumferential heat loss and no contact resistance.

Thermal Apparatus

Some general design guidelines were established to ensure acceptable results. The thermal conductance k/L of both the reference and test materials must be similar within one order of magnitude in order to ensure adequate temperature gradients within the material. Cross-sectional area must be uniformly maintained along the stack

so as to ensure 1-D heat flow. The reference materials must be sufficiently strong enough to withstand an applied load and resist deformation. All of these guidelines had to be considered in designing the system apparatus. Figure 6 shows the general apparatus layout used for experiments.

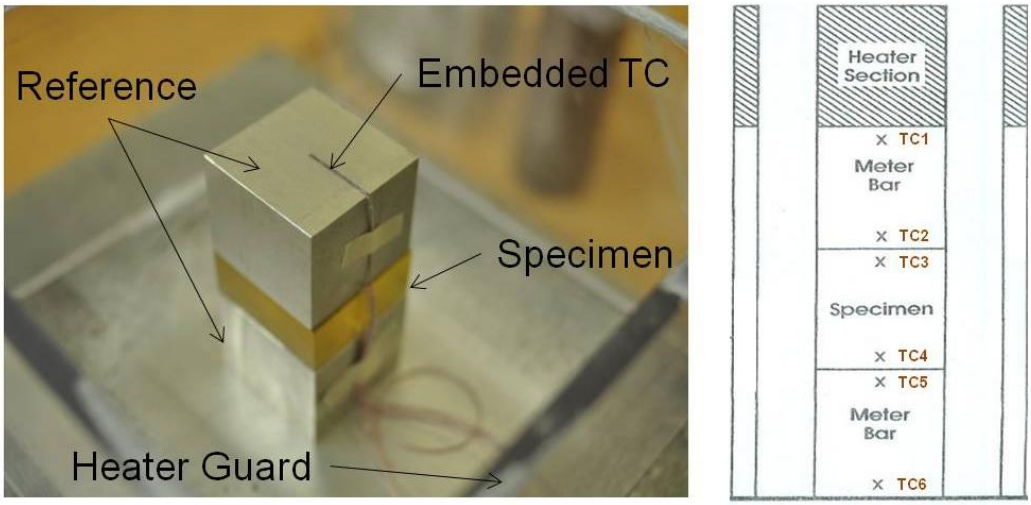

Figure 6 – Experimental thermal apparatus (left) and schematic (right)

Macor, a machineable glass-ceramic, was chosen as the reference materials for its strength and thermal properties. With a thermal conductivity of 1.4 W/mK, it is a close match to epoxy's rated value of 0.3 W/mK. The thermal conductance can further be matched by staggering the relative length of each material. The dimensions of the Macor were chosen to be 1" x 1" x 1" (24.5 mm x25.4 mm x 25.4 mm) resulting in thermal conductance of 54.4 W/m^2K. Dimensions of the epoxy composites were 1" x 1" x ½" (25.4 mm x 25.4 mm x 12.7 mm) with a thermal conductance of 23.6 W/m^2K, which is well within the same order of magnitude of the Macor.

The heater consists of two 75W cartridge heaters embedded within a block of 316 stainless steel with dimensions of 1.25" x 1.25" x 0.7" (31.75 mm x 31.75 mm x 17.8

mm). A 30 AWG Type-T thermocouple was embedded half way into the stainless body in order to run closed loop control of the heater temperature. The heat sink consisted of a large block of aluminum. Thermally conductive grease was used between all specimen and reference interfaces to ensure minimal contact resistance and sufficient heat flow from the heater and into the sink.

Insulation was a critical factor in minimizing circumferential heat loss of the stack. Insulation had to be stable over the specified temperature range of 20 -120 °C and have a low thermal conductivity. Thermal Products' alumina-silica-zirconia S-Durablanket 2600 thermal blanket was used as insulation for its extreme thermal stability and low thermal conductivity of 0.04 W/mK. The blanket was wrapped around the specimen circumferentially to a thickness of approximately 3" (76.2 mm).

Six thermocouples, with two in each material, of type-T 30 AWG were used to obtain temperature gradient information. Notches with dimensions of 0.04" x 0.04" x 0.5" (1.016 mm x 1.016 mm x 12.7 mm) were machined onto both top and bottom surfaces of each material in order to embed the thermocouple near the material center. Electronics grade silicon was used to embed the thermocouples into their respective notches.

Temperature gradient data from the array of thermocouples was transferred through an interfacing unit and then to a computer program called Tracer DAQ via USB. All thermocouples were checked for proper function and calibrated prior to every experiment using Instacal software.

As previously shown, the stack was assembled in a reference-specimen-reference configuration. It should be noted that the labeling of thermocouples as TC1-TC6 as

seen in figure 6 will be carried on in the discussion. The stack was placed between the heater and heat sink with thermally conductive paste between all interfaces. The insulation was then placed around the specimen with a Plexiglass guard box containing it (see figure 7). In order to ensure sufficient contact between all interfaces, the stack was lightly compressed between 50-100 N by the Instron head. A macor spacer with a height of 0.43" (11mm) was placed between the heater and Instron head to minimize unnecessary heat transfer away from the stack. A 110°C was applied to the top of the stack by the heater while the aluminum heat sink maintained room temperature of approximately 23°C. After reaching thermal equilibrium, the thermal conductivity of the specimen was calculated using equation 5.

The stack was then quasi-statically compressed at an extension rate of 0.08 mm/min, translating to a strain rate of 0.00009 s^{-1}. Figure 7 shows the thermo-mechanical apparatus. Total strain of approximately 30 percent was recorded. The changing thermal gradient was monitored in real time and is proportional to the thermal conductivity change.

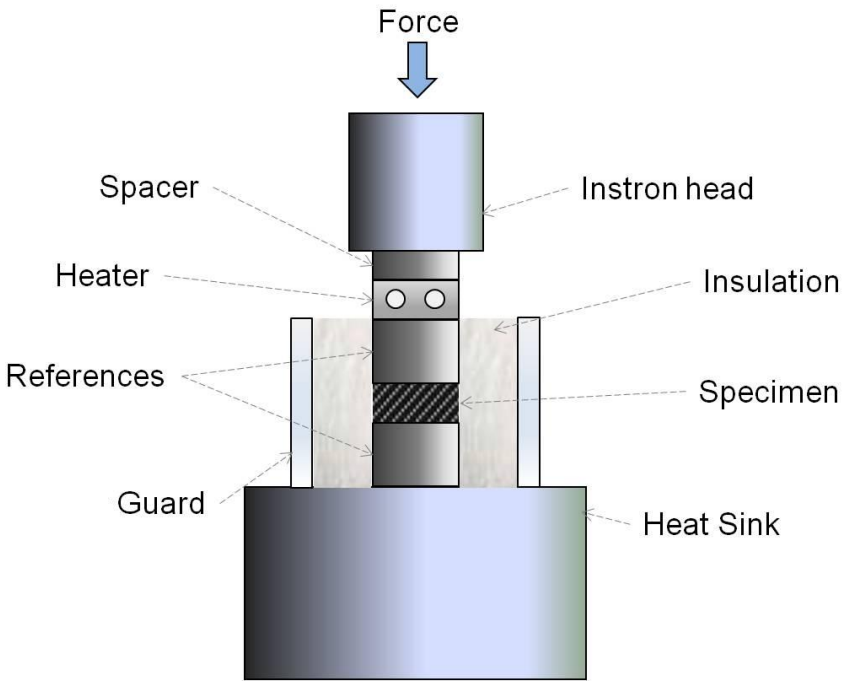

Figure 7 – Thermomechanical apparatus under quasi-static loading

The total strain obtained from this experiment reflects a coupling of strain of the specimen, reference materials, and heater. Although the references and heater were chosen to be at least an order of magnitude stronger than our specimen, all sources of error had to be accounted for. Strain of the specimen was extracted by characterizing load as a function of strain of the reference and heater materials and then using those correlations to subtract from the total strain, thus leaving only the specimen strain value. Quantitatively,

$$\varepsilon_s = \varepsilon_{total} - \varepsilon_m(P) - \varepsilon_{ss}(P) \quad (6)$$

where ε_s is the specimen strain, ε_{total} is the total stack strain, $\varepsilon_m(P)$ is the strain of the macor as a function of load,P, and $\varepsilon_{ss}(P)$ is the strain of the stainless steel as a

function of load. The extracted specimen strain was then correlated with the change in thermal conductivity.

CHAPTER 4

RESULTS & DISCUSSION

Rubber-reinforced CNT/Epoxy - Quasi-static

Compression experiments were conducted in order to characterize the electrical response of each rubber-reinforced CNT/epoxy case (0 phr, 10phr, 20phr, 30phr). CNT weight content was held at a constant 0.2 wt% for all cases. All compression experiments were conducted with an applied extension rate of 0.15mm/min. All experiments were halted between 20-25% strain and with visible barreling of the specimen.

The electrical response with respect to strain from the 0, 10, 20, and 30 phr cases are shown in figures 8, 9, 10, and 11, respectively. Each specimen was compressed to 20% strain in which visible bulging began to occur. The damage evolution of these composites were divided into three distinct stages and analyzed (Figure 12).

The first stage defines the linear elastic region and shows the onset of electrical response. This initial electrical response indicates that the CNT network and epoxy are not yet undergoing any significant reorientation or bond damage, rather the nanotube network and epoxy matrix are simply being elastically compressed. This compression increases the material density and in turn increases the effective nanotube density (nanotubes per unit volume) and corresponds to a net increase in nanotube-nanotube contact and overlap, thus allowing more paths for charge carriers to flow. Stage I strains remained virtually unchanged for all rubber loadings with the elastic region

lasting until approximately 4% in all four cases. Electrical response was also virtually the same among all cases with a resistance drop of about 12%.

Stage II occurs after the elastic limit of Stage I. This stage showed the most significant changes among the four cases. As the specimen is compressed beyond its elastic limits, the inter-nanotube and epoxy bonds begin to break and significantly reorient themselves. The number of nanotube bond formations far exceeds the number of broken bonds in this stage, thus allowing a dramatic net increase in nanotube network contact area. This drastic reorientation of the nanotube network results in an increase in inter-nanotube contact. Because the nanotubes are the sole entity of electrical transport in the composite, a dramatic decrease in resistance is observed.

Stage III corresponds to the final stage of electrical response denoted by a shift from decreasing to increasing resistance. Now that the material is far into the plastic region, further compressive energy results in internal compressive and shear damage of the specimen manifesting as micro-cracks and bulging. These cracks and voids gradually disrupt and break the inter-nanotube bonds within the nanotube network and thus cause the electrical resistance to plateau and proceed to increase until catastrophic failure.

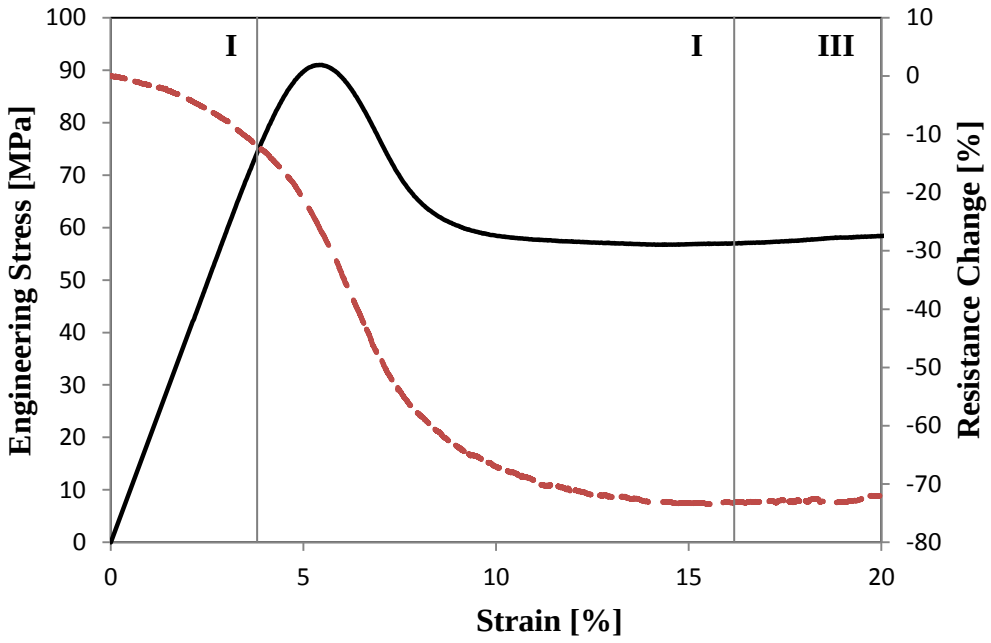

Figure 8 – Mechanical (left axis) and electrical (right axis) response of CNT/epoxy with a rubber content of 0 phr

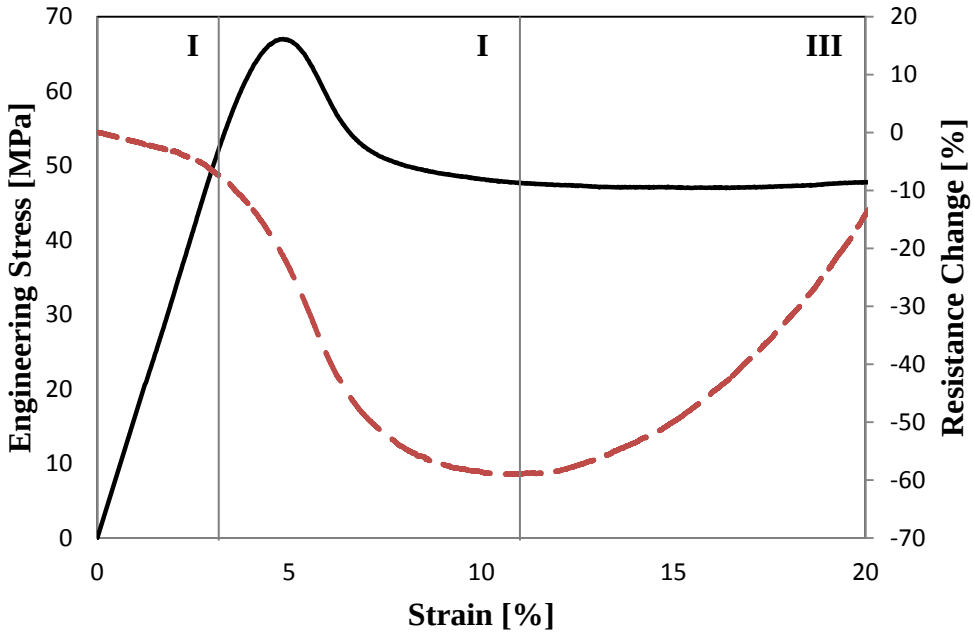

Figure 9 – Mechanical (left axis) and electrical (right axis) response of CNT/epoxy with a rubber content of 10 phr

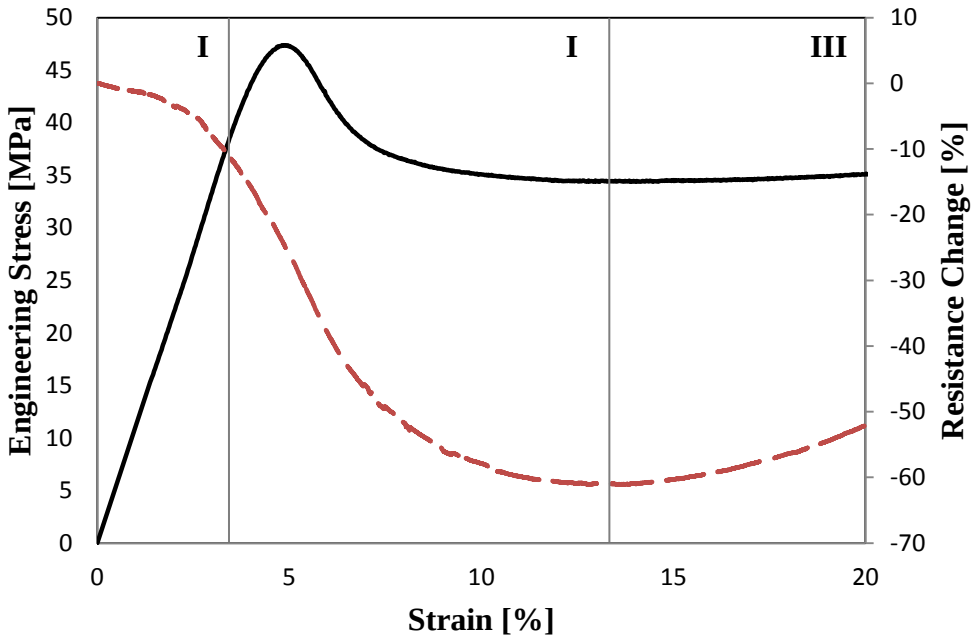

Figure 10 – Mechanical (left axis) and electrical (right axis) response of CNT/epoxy with a rubber content of 20 phr

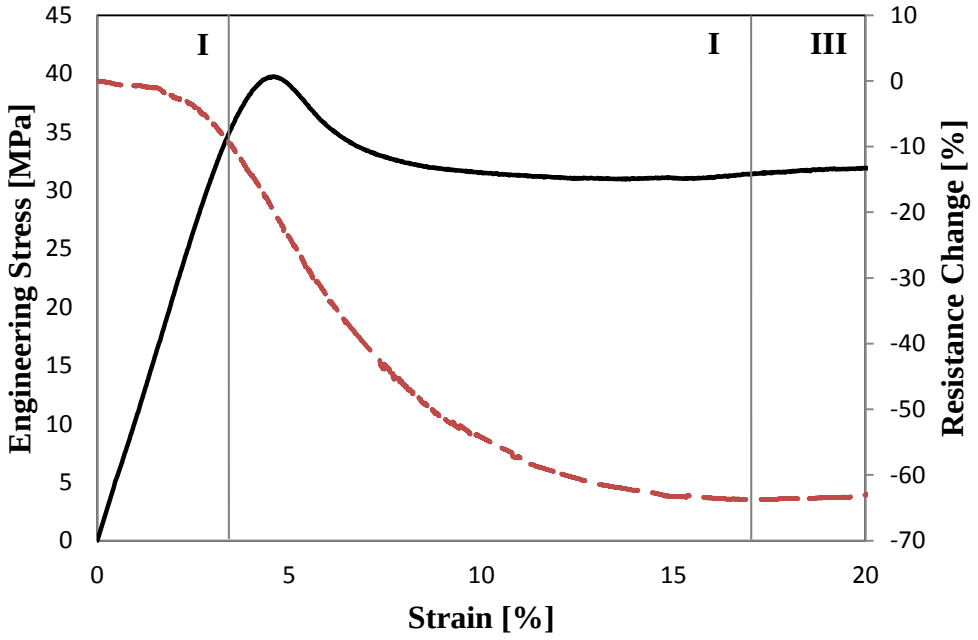

Figure 11 – Mechanical (left axis) and electrical (right axis) response of CNT/epoxy with a rubber content of 30 phr

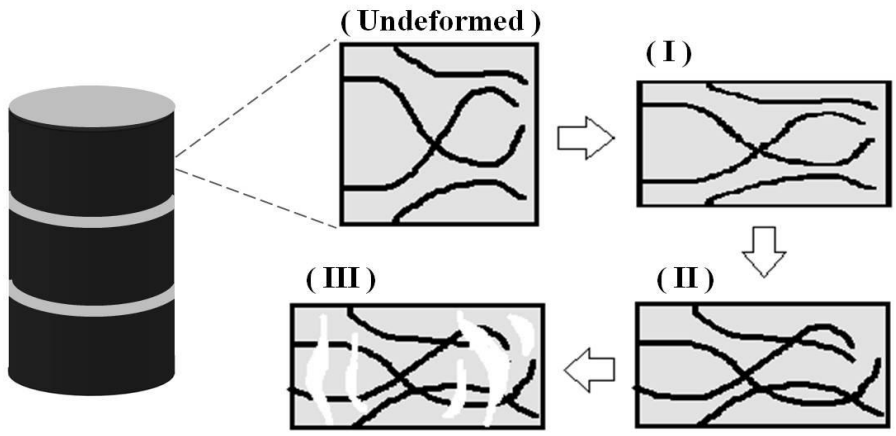

Figure 12 – Stages of nanotube evolution starting with the undeformed state to the various stages of compression (I, II, III)

Important information on the mechanical and electrical properties can be extracted from these results. Figure 13 shows a comparison of the mechanical response, plotted as engineering stress, with respect to strain of the four cases. It can be seen immediately that the composite becomes much softer and weaker with increasing rubber content. Key points of emphasis are the decreasing Young's modulus and peak stress values. It can also be seen that the strain at which peak stress occurs decreases slightly with increasing rubber content. These results are to be expected in approximate accordance with the rule of mixtures.

Figure 14 shows a comparison of the electrical response, plotted as the change in resistance, with respect to strain in all four cases. The 0 phr case showed the highest peak resistance change of 73% as well as the broadest U-shape curve with very wide plateauing. With the addition of 10 phr rubber, the response shrunk to a lower peak change of 59% and to a much narrower U-shape curve. Subsequent addition of 20 and 30 phr led to increases in peak resistance of 62% and 64%, respectively, and occurring at increasingly later strains. The broadness of the U-shape of the 20 and 30 phr cases

also increased proportionally. Key mechanical and electrical values were tabulated in Table 1. It should be noted that the maximum resistance change (ΔR/R) and ΔR/R @ 20% strain columns together help to give some quantification of the broadness of the U-shape.

The broadening effect of the electrical response that appears in the 10, 20, and 30 phr specimens can be attributed to the rubber's influence to effectively rubberize the material to withstand higher strains and delay the onset of micro-cracking and internal damage. This delay is seen with increasing peak resistance changes and broader U-shape. This does not carry over to the plain epoxy case, where by following the same trend, the peak electrical response should be less with a sharper U shape than the 10 phr case. This can be explained when taking the CNT/epoxy/rubber interaction and functionalisation into account. Because the 0 phr epoxy/CNT case showed the highest mechanical strength as well as the highest change in resistance and broadest U-shape electrical response, it can be deduced that the CNT/epoxy exhibited the strongest matrix-filler interactions of the bunch. The subsequent cases of 10, 20 and 30 phr show a much weaker interfacial interaction compared to the 0 phr case, but an interfacial increasing interaction relative to 10 phr as displayed by the improving electrical response and damage delay.

Rubber content (phr)	Youngs Modulus (GPa)	Peak stress (MPa)	Electrical transition strain (%)	Max ΔR/R (%)	ΔR/R @ 20% Strain (%)
0	1.98	91	16	73	72
10	1.66	67	11	59	15
20	1.18	47	13	62	53
30	1.07	40	17	64	63

Table 1 – Mechanical and electrical data from quasi-static experiments

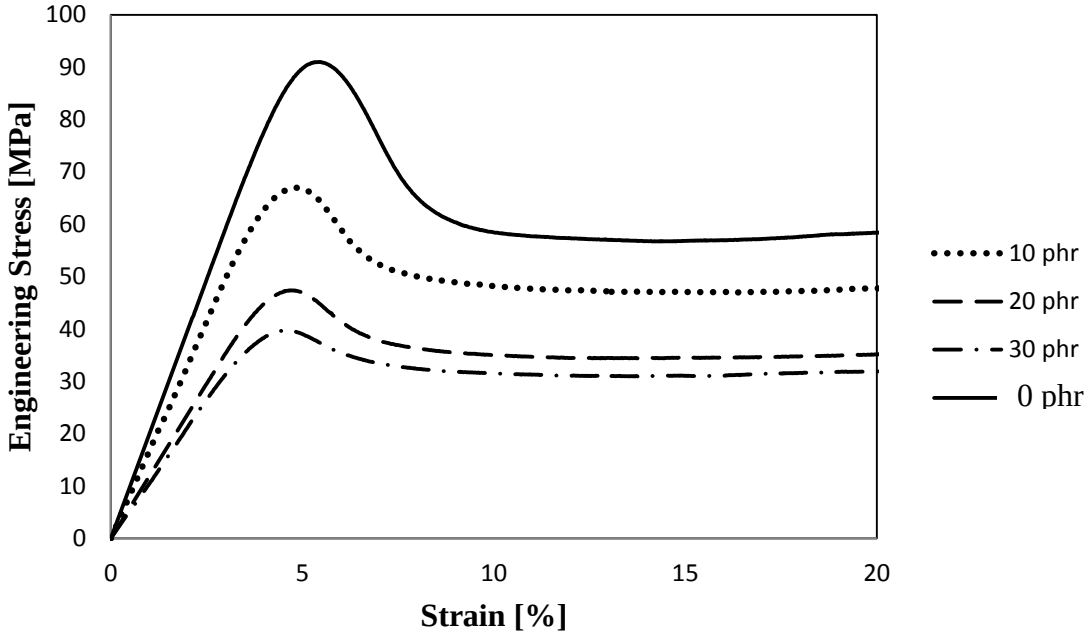

Figure 13 – Mechanical response of CNT/Epoxy with rubber loadings of 0, 10, 20 and 30 phr

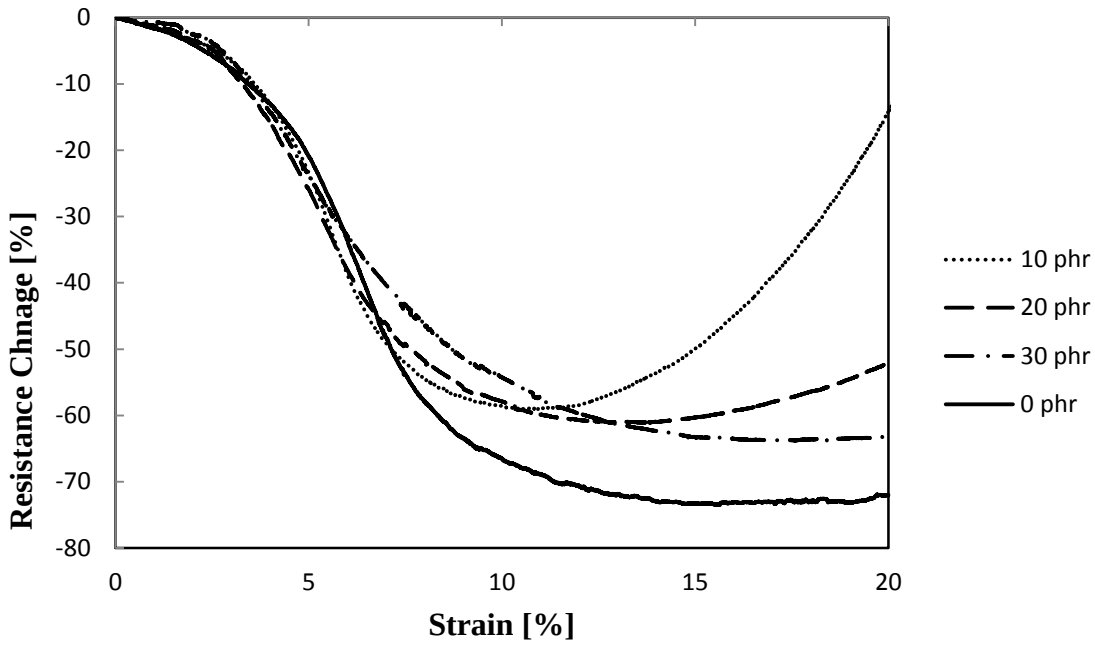

Figure 14 – Electrical response of CNT/Epoxy with rubber loadings of 0, 10, 20 and 30 phr

Rubber-reinforced CNT/Epoxy - Dynamic

Dynamic experiments were conducted in order to characterize the electrical response of each material case (0 phr, 10phr, 20phr, and 30phr). CNT weight content was held at a constant 0.2 wt% for all cases. Dynamic compression experiments were conducted using an SHPB apparatus with applied strain rates ranging from 700-1000 s^{-1}. Force equilibrium was confirmed in all experiments on both faces of the specimen. All experiments were executed with a 16" striker bar launched at a pressure of 125 psi.

The electrical response with respect to strain from the 0, 10, 20, and 30 phr cases are shown in figures 15, 16, 17, and 18. Each specimen was compressed to 12-17% depending on the strength of the material. With that said all specimens were loaded

well into the plastic region of deformation but did not experience the electrical plateauing and subsequent resistance increase as in the quasi-static results.

The damage evolution of these composites can be divided into two distinct stages with similar findings as in the quasi-static experiments. The first stage again defines the linear elastic region and shows the onset of electrical response. This resistance change is nearly identical with that of quasi-static data and indicates that the CNT network and epoxy are not yet undergoing any significant reorientation, but rather elastic compression. An increase in inter-nanotube contact is creating a more integrated electrical network and thus allowing more paths for charge carriers to flow. Stage I strains remained virtually unchanged with the elastic region lasting until approximately 4% in all four cases. Electrical response was also virtually the same among all cases with a resistance drop of about 12%.

Stage II occurs at the onset of yielding of the specimen. This stage once again showed the most significant changes among the four rubber loadings. This stage spans the remaining strain. It should be noted that due to the limitations placed on this set of dynamic experiments, and therefore on the maximum strain achieved, peak resistance change values may not have been fully realized. With that said, specimens were still deformed well into the plastic region and important information could still be extracted. Resistance again decreased between 60-70% among all cases in this stage but with no defined trend among the different rubber loadings. Due to the nature of dynamic experiments and material strain dependence, some variation is expected. As with quasi-static data, the specimen is compressed beyond its elastic limits and the inter-nanotube and epoxy bonds begin to break and significantly reorient themselves

allowing a stark increase in nanotube network contact area, and thus increasing conductivity.

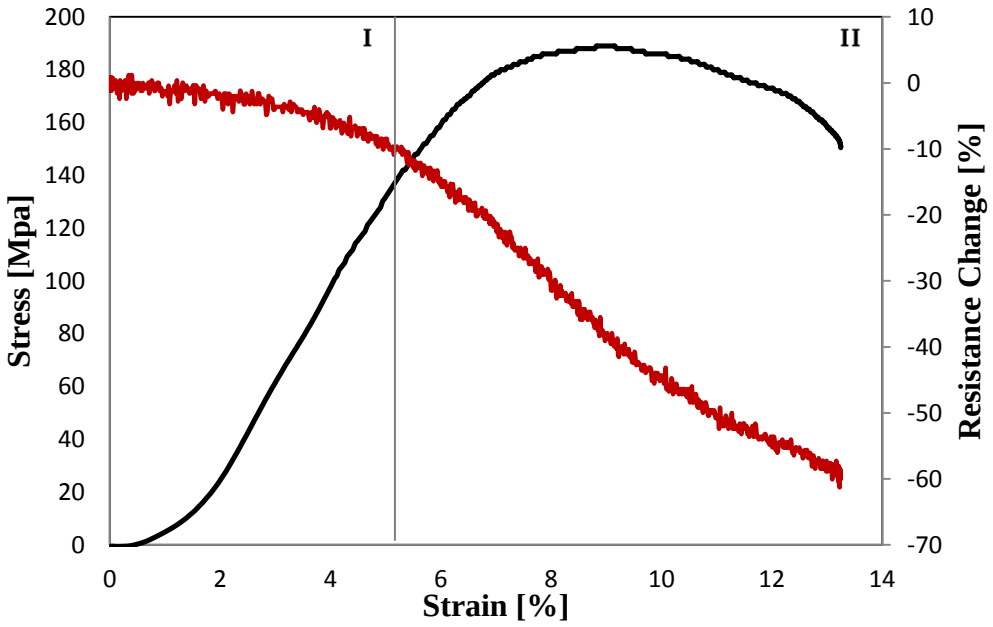

Figure 15 – Dynamic mechanical and electrical response of CNT/epoxy with a CTBN rubber content of 0 phr

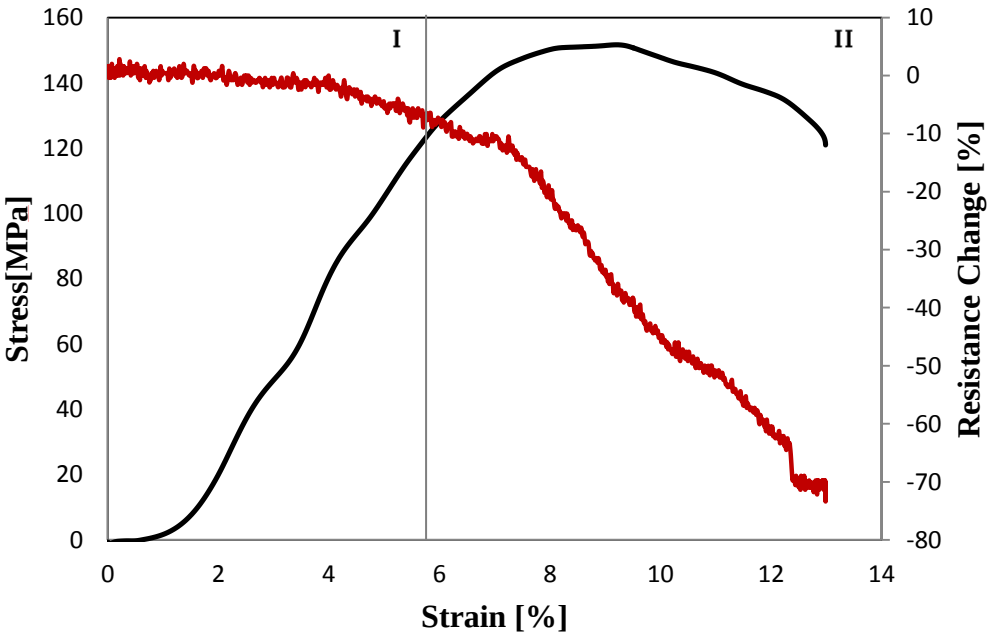

Figure 16 – Dynamic mechanical and electrical response of CNT/epoxy with a CTBN rubber content of 10 phr

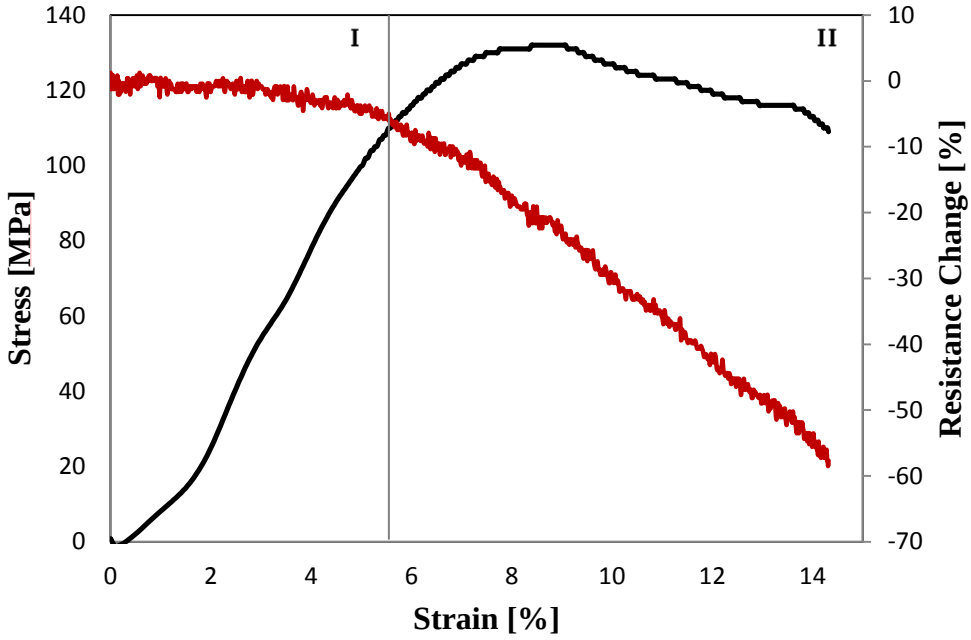

Figure 17 – Dynamic mechanical and electrical response of CNT/epoxy with a CTBN rubber content of 20 phr

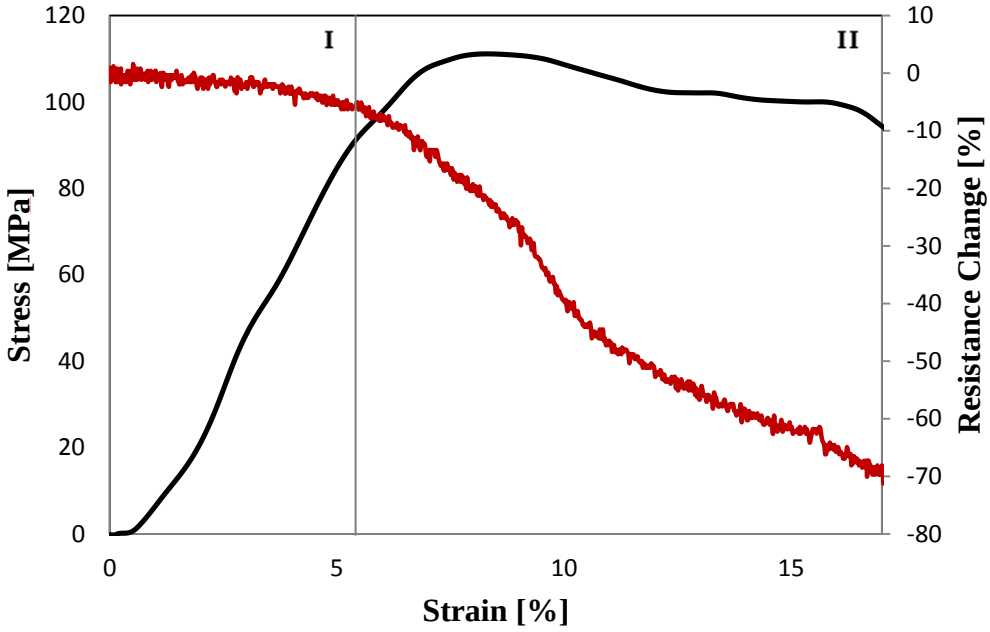

Figure 18 – Dynamic mechanical and electrical response of CNT/epoxy with a CTBN rubber content of 30 phr

Important information on the mechanical and electrical properties can be extracted from these results. Figure 19 shows a comparison of the mechanical response, plotted as engineering stress, with respect to strain of the four cases. As with quasi-static results, it can be seen that the composite becomes much softer and weaker with increasing rubber content. Decreasing Young's modulus and peak stress values once again indicate softening of the material. It can also be seen again that the strain at which peak stress occurs decreases slightly with increasing rubber content. A strong strain rate dependence can be seen in this material with 50-70% increases in Young's modulus 100-175% increases in peak stress.

Figure 20 shows a comparison of the electrical response, plotted as the change in resistance, with respect to strain in all four cases. It can be seen here that the change in resistance up to the plotted 13% strain are all relatively the same (with the exception of the 10 phr case, although this fell within the average deviation). The same resolution as quasi-static data was not obtained due to short event (200 μs) and the limit in acquisition frequency. With that said, these results show a very similar initial response for all four cases, but further inquiry would be necessary to determine the overall U-shape and peak resistance change values. Some key mechanical and electrical parameters from dynamic experiments are outlined in Table 2.

Rubber content (phr)	Youngs Modulus (GPa)	Peak stress (MPa)	Max ΔR/R (%)	Max Strain (%)
0	2.95	189	60	13
10	2.42	156	72	13
20	2.12	133	60	14
30	1.82	111	70	17

Table 2 - Mechanical and electrical data from dynamic experiments

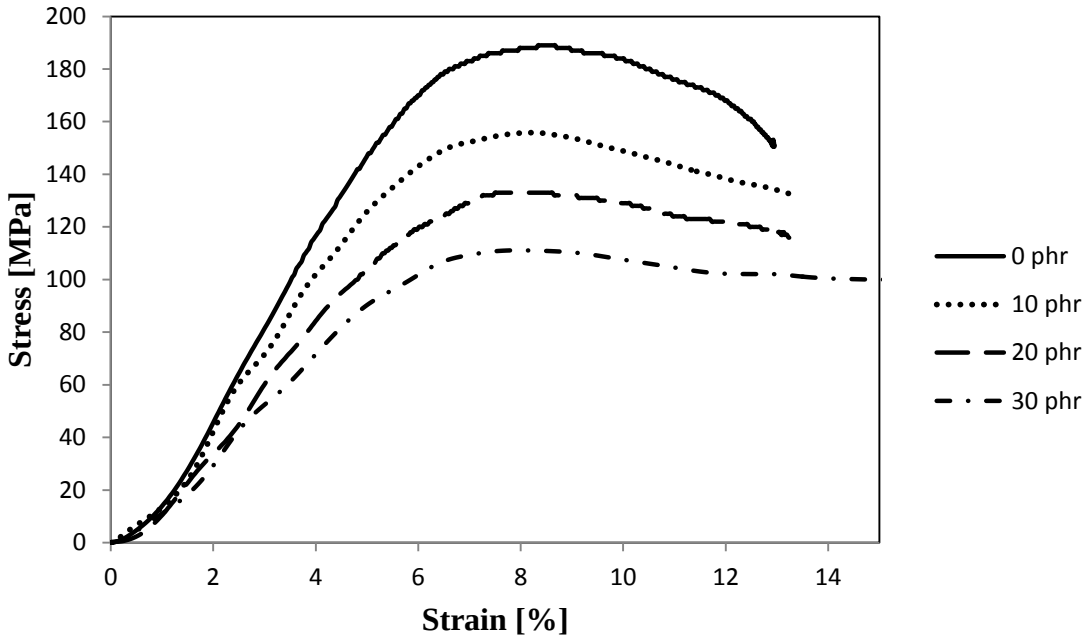

Figure 19 – Dynamic mechanical response of CNT/Epoxy with CTBN rubber loadings of 0, 10, 20 and 30 phr

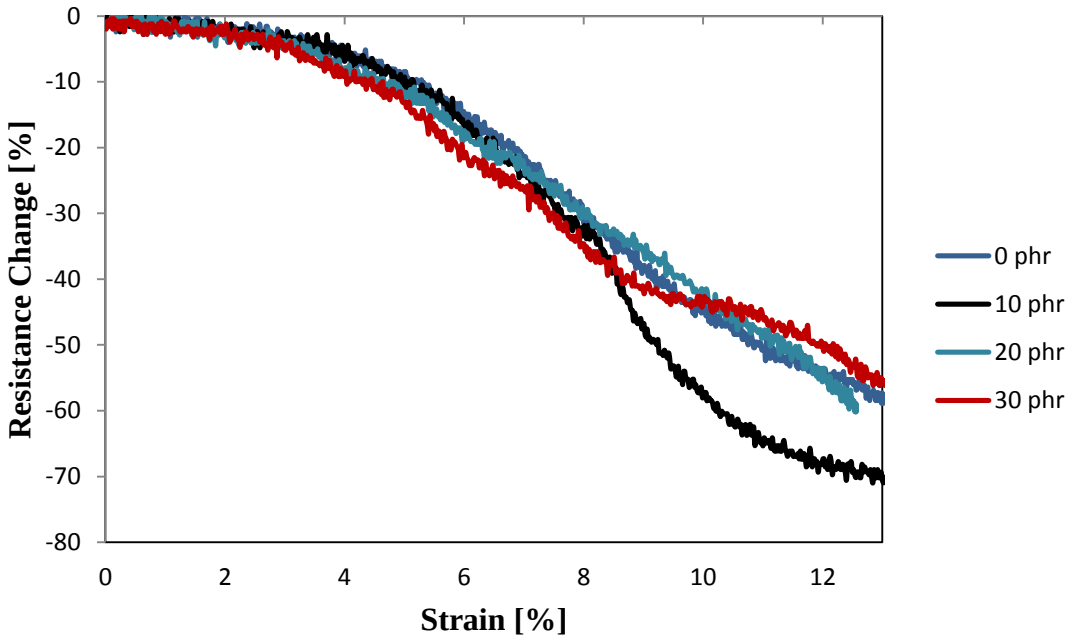

Figure 20 – Dynamic electrical response of CNT/Epoxy with CTBN rubber loadings of 0, 10, 20 and 30 phr

Figures 21, 22, 23, and 24 show the resistance change with respect to time for the 0, 10, 20, and 30 phr cases, respectively. All plots were supplemented with high-speed images obtained during the experiment. In each picture, on the right and left are the incident and transmitted bars both sandwiching the cylindrical specimen in the center. It can be seen from the images that all specimens showed a minimal amount of bulging which attributes to the effectiveness of the conductive lubricant. These images also confirm that these specimens were properly loaded uniformly along their axial direction and that no specimen was catastrophically loaded.

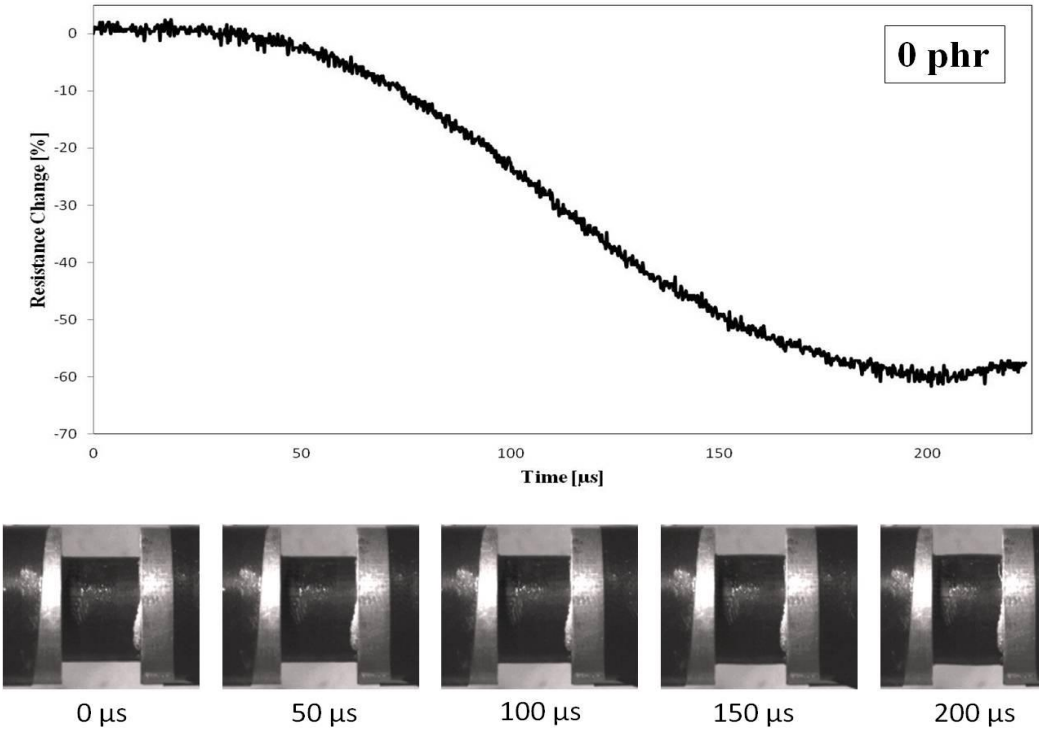

Figure 21 – Dynamic electrical response of 0 phr rubber CNT/epoxy composite with high-speed images of deformation

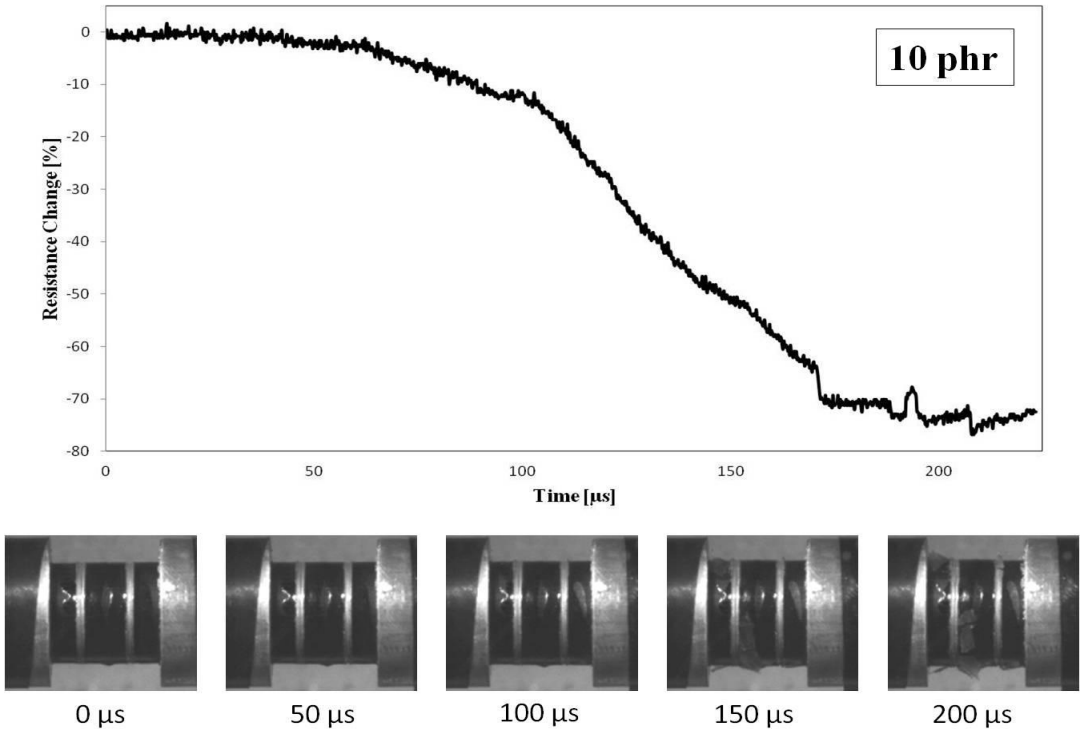

Figure 22 – Dynamic electrical response of 10 phr rubber CNT/epoxy composite with high-speed images of deformation

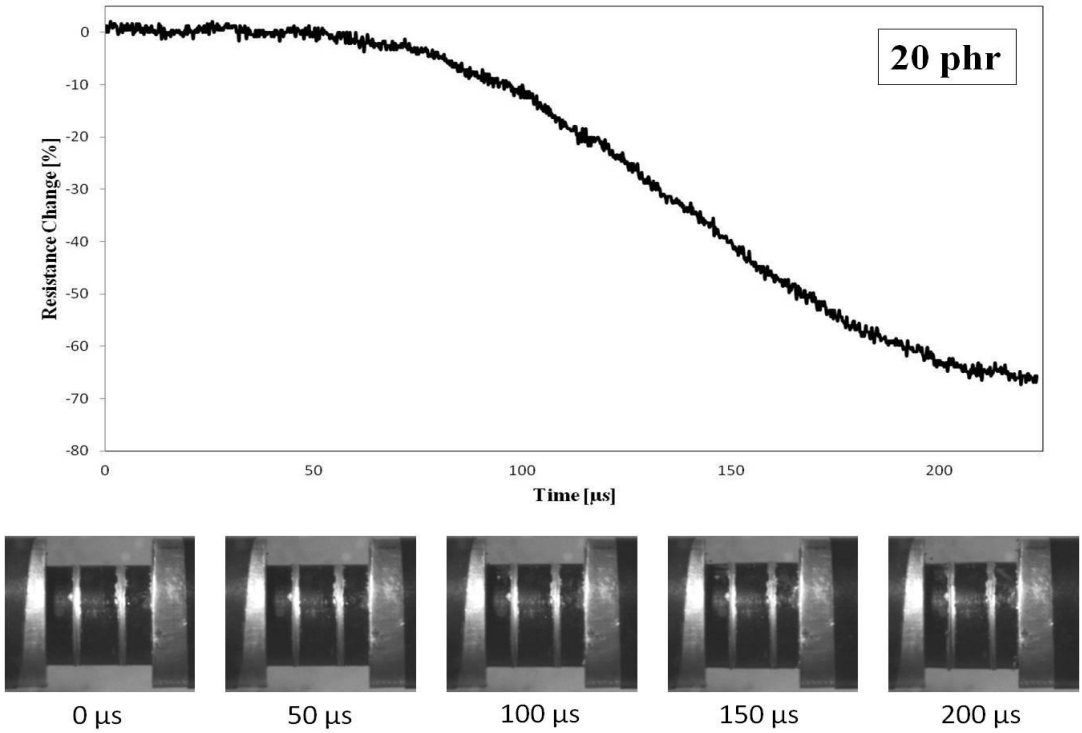

Figure 23 – Dynamic electrical response of 20 phr rubber CNT/epoxy composite with high-speed images of deformation

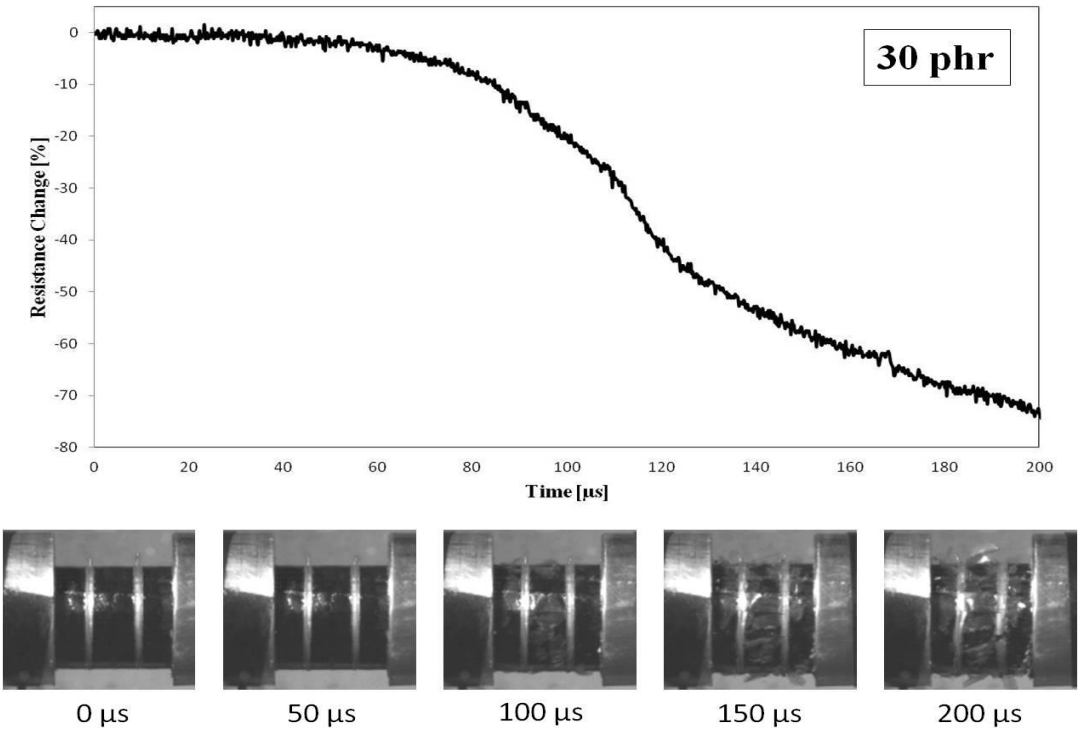

Figure 24 – Dynamic electrical response of 30 phr rubber CNT/epoxy composite with high-speed images of deformation

CNT/Epoxy - Thermal Percolation

Thermal experiments were conducted in order to first characterize how the thermal conductivity changes with respect to CNT filler content. All experiments were executed by applying a temperature gradient of approximately 87°C across the stack with a heater temperature of 110°C and heat sink at 23°C corresponding to room temperature. Thermal equilibrium was reached after approximately 80 minutes. Figure 25 shows an example of the transient response at each thermocouple site located in the stack. Thermal conductivity values were calculated, using the top, bottom, and averaged heat fluxes along the stack, for each CNT loading using the respective steady state temperature values and plotted in figure 26.

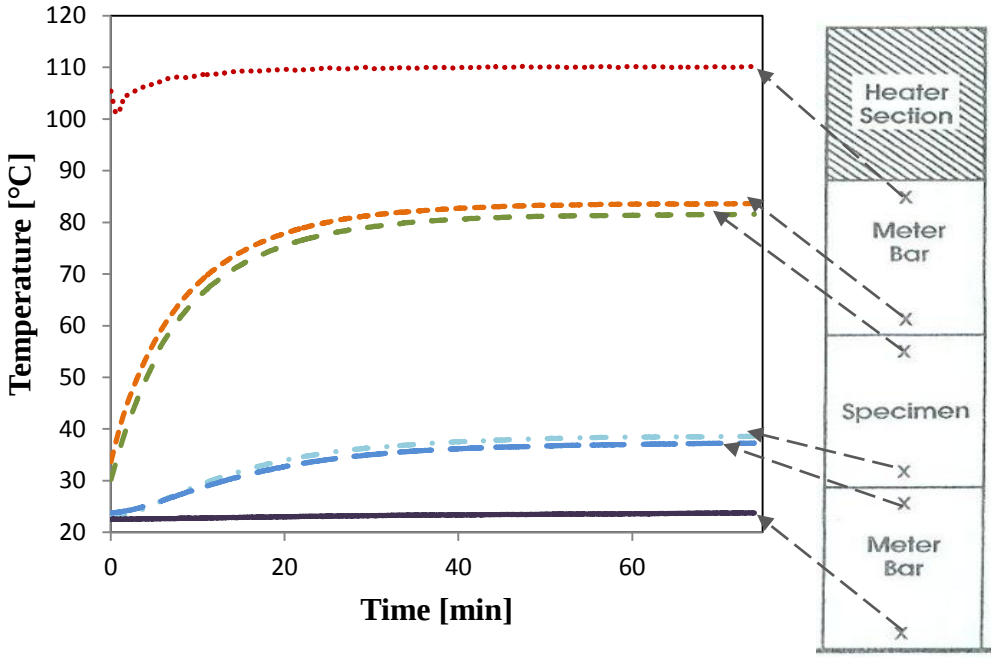

Figure 25 – Transient thermal gradients of top reference material (TC1, TC2), specimen (TC3, TC4), and bottom reference material (TC5, TC6)

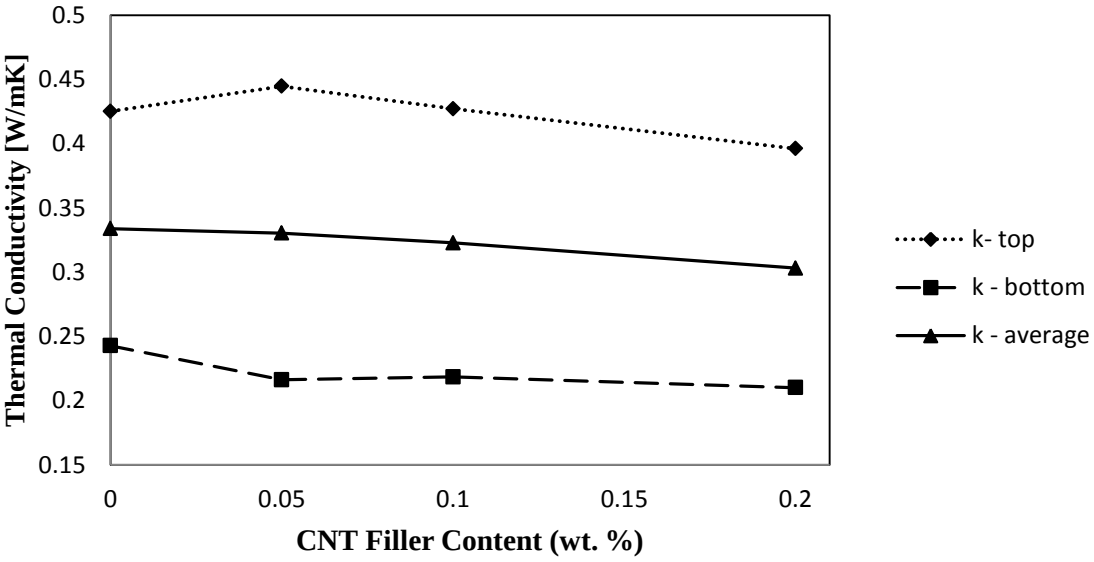

Figure 26 – Thermal conductivity with respect to CNT filler content (percolation study)

It should be noted that the difference in heat flux, and respective thermal conductivity, from top to bottom corresponds to a fairly significant heat loss as they should be the same in a one-dimensional system. Despite the error, important information can still be deduced. It can be seen from these values that there was very little change in thermal conductivity with increasing loadings of CNT. This is in contrast to previous findings of conductivity increases. However, Moisala et al. (2006) saw similar decreasing values with SWCNT/epoxy. It is believed that this decrease is not due to damaged nanotubes or the lack of a percolation network as both were confirmed by previous electrical conductivity work with identical fabrication processes. This result points to a poor interaction between the nanotubes and epoxy leading to a large interfacial resistance between the two. Because phonons are the dominant mechanism of thermal transport in CNT, the interfacial resistance between the CNT and epoxy will cause poor phonon coupling between the two and thus thermal transport is poorly transferred. Furthermore, it is possible that the phonon vibrations from nanotube to nanotube are quickly dampened due to a lack of rigid connection between the two, as is necessary for the transmission of any vibrational information. Phonon transfer may also be greatly dampened by the epoxy matrix itself.

CNT/Epoxy - Quasi-static Thermal Conductivity

After reaching thermal equilibrium, a constantly increasing quasi-static compressive load was applied to the specimen with an extension rate of 0.08 mm/min and corresponding strain rate of $0.00009\ s^{-1}$. Using such a low strain rate allowed us to assume minimal shifting from thermal equilibrium.

Figure 27 shows the transient temperature profile and corresponding change in thermal conductivity of the plain epoxy specimen. The initial instability can be attributed to the top thermocouple, TC1, not reaching the target heater temperature of 110°C, although it should be noted that the stack was in equilibrium prior to quasi-static loading. The transient increase to 110°C is due to the increase in contact force and overall decrease in contact resistance. Peak stresses showed approximately 55 MPa which is noticeably weaker than established values at room temperature. This is to be expected as the upper portion of the specimen passed the glassy temperature, T_g, of 64°C. This also leads to noticeable bulging in the upper specimen region at high strains and thus creates increasing heat loss and error.

Thermo-mechanical loading results on average show zero change in thermal conductivity. This result is to be expected as the ratio of temperature difference to specimen length for plain epoxy should stay constant and therefore result in no change in thermal conductivity.

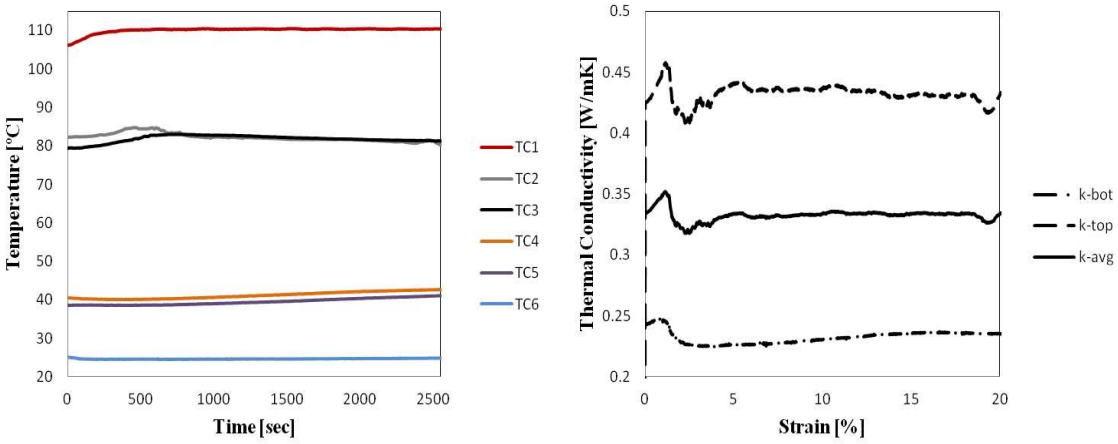

Figure 27 – Thermal gradient (left) and thermal conductivity versus strain of plain epoxy under quasi-static compression

Figure 28 shows the transient temperature profile and corresponding change in thermal conductivity of the 0.05 wt.% CNT/epoxy specimen. The temperature distribution at the top and bottom thermocouples, TC1 and TC6, stayed reliably constant for the entirety of the experiment, as expected. Thermal conductivity results however yielded some important information. Firstly it can be seen that the thermal conductivity as calculated from the temperature gradient appears to be decreasing with increasing strain. While this data may have some validity to it, it should be first noted that there was a source of increasing error as the experiment progressed, and the same can be said for the remaining CNT/epoxy loading experiments (figures 29, 30).

This progressive error was due to the overall weakening of the specimen at the specified temperature gradient and the resulting bulging that occurred. This bulging was noted in the plain epoxy case, but bulging occurred much earlier in the CNT/epoxy cases. This early-stage bulging agreed very much with mechanical data – peak stresses were an order of magnitude lower than that of plain epoxy, with values of approximately 3.1 MPa for all CNT specimens.

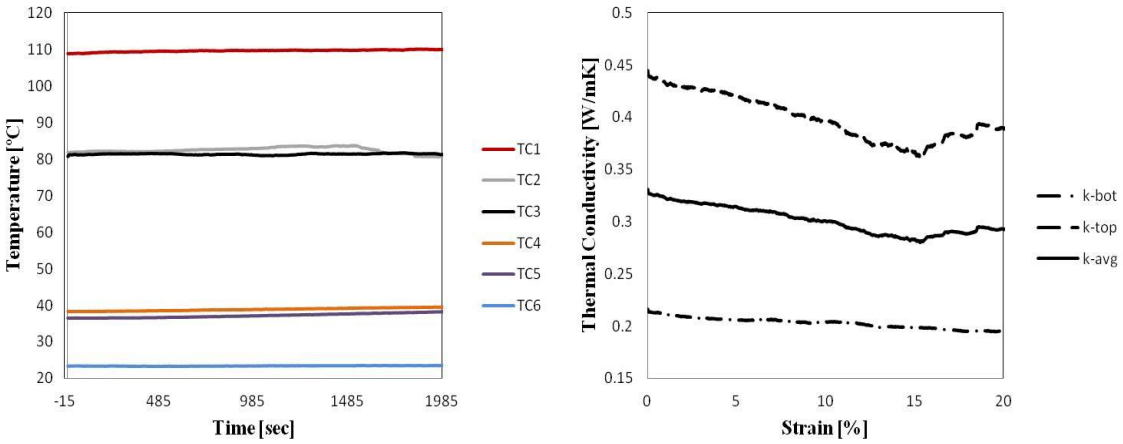

Figure 28 – Thermal gradient (left) and thermal conductivity versus strain of 0.05 wt% CNT-embedded epoxy under quasi-static compression

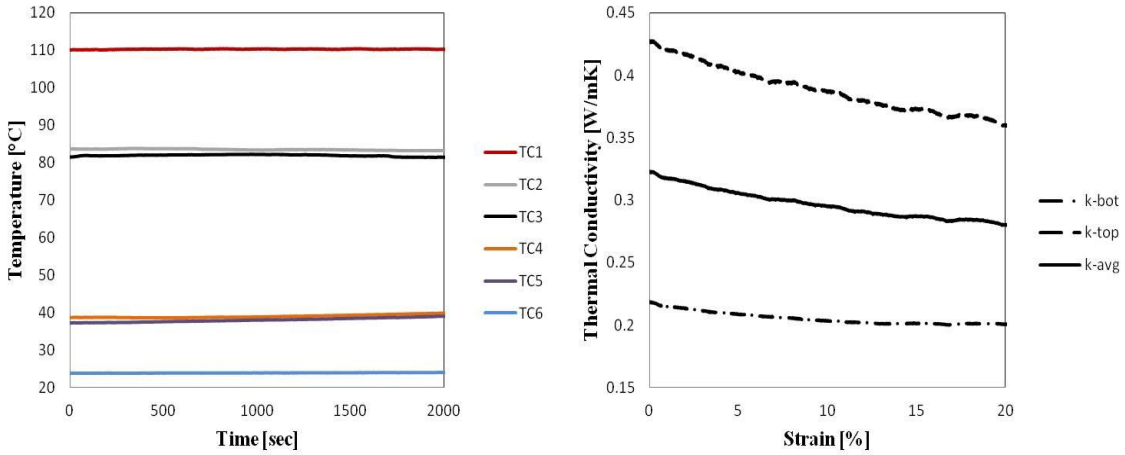

Figure 29 – Thermal gradient (left) and thermal conductivity versus strain of 0.1 wt% CNT-embedded epoxy under quasi-static compression

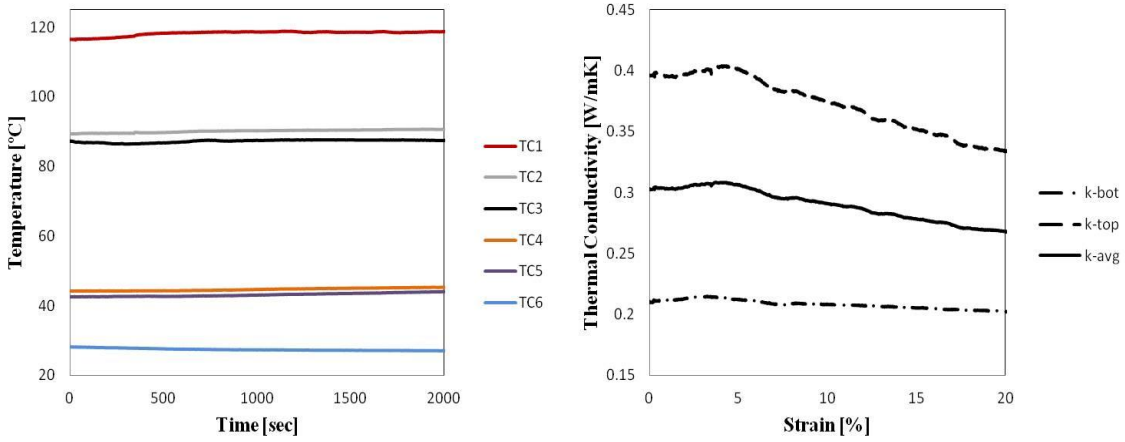

Figure 30 – Thermal gradient (left) and thermal conductivity versus strain of 0.2 wt% CNT-embedded epoxy under quasi-static compression

With this critical information, it can be concluded that at elevated temperatures, the use of CNT as a filler in an epoxy matrix dramatically decreases the strength of the composite. It was concluded from the percolation study above that the CNT and epoxy were interacting very weakly. This fact is exacerbated at higher temperatures and results in weakening and rapid degradation of the epoxy matrix. Post mortem images (figure 31) show the difference in damage. While the plain epoxy specimen showed

large cracking along the perimeter, the CNT/epoxy specimens showed complete surface decomposition and displayed a crumbling effect on the top surface. It is apparent that this drastic weakening corresponds mostly in the glass transition area, as the lower portion of the specimen did not show such degradation.

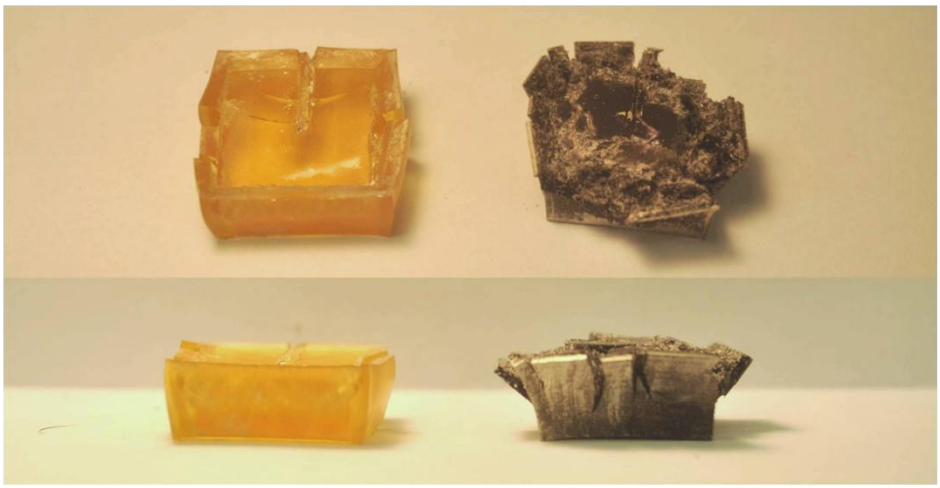

Figure 31 – Post-mortem images of compressed plain epoxy (left) and 0.05 wt% CNT/epoxy (right)

Given the previous information, it can be concluded that the decrease in calculated thermal conductivity as seen in Figures 27, 28, and 29 can be largely attributed to the increase in heat loss due to bulging and deviation from a 1-D heat transfer system. With that said it is still possible that there is a decrease in thermal conductivity with applied load as even lower strains still showed decreases. A possible way to decouple the two mechanisms would be to shift the temperature gradient down so that the specimen remains below the glass transition state. This should result in a significant decrease in bulging and more uniform deformation.

CHAPTER 5

CONCLUSIONS AND FUTURE WORK

This study experimentally investigated the electrical and thermal response of carbon nanotube/epoxy composites under mechanical loading. Valuable information about the influence of rubber reinforcement on the electrical and mechanical response of CNT/epoxy composites was realized. An apparatus and experimental approach was established to investigate the thermal conductivity of unknown materials as well as their response under quasi-static loading. The key findings of this study are presented below.

Quasi-static CNT/Epoxy/CTBN

The introduction of CTBN rubber to the CNT/Epoxy composite showed a progressive weakening of Young's modulus and peak stress with increasing rubber content. The peak change in electrical resistance of 73% was seen in the epoxy sample and also showed the broadest response. The initial addition of rubber at 10 phr led to a stark decrease in electrical response (59%) and also showed the narrowest response. Subsequent loadings of 20 and 30 phr led to a broadening higher peak resistance changes and a broadening of the response curve due to a delay in micro-cracking and material degradation. This characterization opens possibilities of engineering materials to specific desirable properties for a given application.

Dynamic CNT/Epoxy/CTBN

The introduction of CTBN rubber to the CNT/Epoxy composite showed the same progressive weakening of Young's modulus and peak stress with increasing rubber

content as seen in quasi-static experiments. A strong mechanical strain rate dependence was observed in all cases. Electrical response however did not show any significant strain dependence and responded very similarly to quasi-static loading. Due to the experimental constraints and strain limits, a full plastic response was not realized and would be worth further inquiry to see the resistance transition.

Thermal Conductivity

Thermal conductivity values taken at CNT weight percentages of 0, 0.05, 0.1, and 0.2 yielded no significant change in thermal conductivity. The small observed decrease is within calculable error. This lack of change can be attributed to the fact that the dominant mechanism of conduction in CNT is acoustic phonons, and therefore vibrational information is quickly dampened weak nanotube-epoxy interactions. It should also be noted that due to the nonlinear temperature gradient, and its correspondence with heat loss, absolute calculated values show error with values of 0.33 W/mK as compared to literature values of 0.24 W/mK.

These losses could be addressed by further optimization of insulation and the implementation of a heater guard surrounding the insulation. Another way to minimize radial heat loss are to reduce the length of the reference materials and specimen so that the radial surface area is reduced.

Quasi-static Thermal Conductivity

While the results of the compressive quasi-static thermal experiments cannot be considered absolute, they yielded some useful preliminary information for further investigation. Because the upper half of the specimen gradient was past the glass

transition temperature, bulging occurred in all specimens. Bulging was especially pronounced in all CNT specimens and occurred much more rapidly and catastrophically than the plain epoxy case. This information coupled with the order-of-magnitude decrease in mechanical strength of the CNT specimens says that the presence of CNT in epoxy above the glass transition temperature dramatically weakens the composite. This is due to an increased degradation of the of the CNT-epoxy interface. This likely occurs from increasing molecular oscillations that break the interfacial bonds more rapidly. With that said, the general results showed that little to no change in thermal conductivity occurred under an applied load. Ultimately, this agrees with the percolation study in that little to no heat is being transferred by the CNT network due to vibrational damping.

Future revisions can be made to the experiment to obtain more information. Firstly, as discussed, an approach to reduce heat loss along the stack is of most importance. The implementation of a heater guard and reduction in radial surface area of the reference materials and specimen would dramatically reduce heat loss and increase accuracy. Furthermore, under quasi-static loading, lowering the gradient within the specimen to below the grass transition temperature of 64°C would dramatically decrease bulging and yield more accurate results.

BIBLIOGRAPHY

Alexopoulos, N.D., Bartholome, C., Poulin, P., Marioli-Riga, Z., "Structural health monitoring of glass fiber reinforced composites using embedded carbon nanotube (CNT) fibers", *Composites Science and Technology* 70, 2009, pp 260-271

Alexopoulos, N.D., Bartholome, C., Poulin, P., Marioli-Riga, Z., "Structural health monitoring of glass fiber reinforced composites using embedded carbon nanotube (CNT) fibers", *Composites Science and Technology* 70, 2009, pp: 260-271

Allaoui, A., Bai, S., Cheng, H.M., Bai, J.B., "Mechanical and electrical properties of a MWNT/epoxy composite", *Composites Science and Technology* 62, 2002, pp: 1993-1998

Bal, S., Samal, S.S., "Carbon nanotube reinforced polymer composites – a state of the art", *Bull Mater Sci* 30, 2007, pp: 379-86

Balakrishnan, A., Saha, M.C., Tensile fracture and thermal conductivity characterization of toughened epoxy/CNT nanocomposites", *Materials Science and Engineering A 528*, 2011, pp 906-913

Bauhofer, W., Kovacs, J.Z., "A review and analysis of electrical percolation in carbon nanotube polymer composites", *Composites Science and Technology* 69, 2009, pp: 1486–1498

Berber, S., Kwon, Y.K., Tománek, D., "Unusually High Thermal Conductivity of Carbon Nanotubes" *Physical Review Letters 84*, 2000, pp 4613–4616

Breuer, O., Sundararaj, U., "Big returns from small fibers: a review of polymer/carbon nanotube composites", *Polymer Composites* 25, 2004, pp: 630-645

Bryning, M.B., Milkie, D.E., Islam, M.F., Kikkawa, J.M., Yodh, A.G., "Thermal conductivity and interfacial resistance in single-wall carbon nanotube composites*", Applied Physics Letters 87*, 2005, pp 161909 (3pp)

Coleman, J.N., Khan, U., Blau, W.J., Gun'ko, Y.K., "Small but strong: A review of the mechanical properties of carbon nanotube–polymer composites", *Carbon 44, Issue 9*, 2006, pp 1624–1652

Collins, P.G., Avouris, P., "Nanotubes for electronics", *Scientific American* 283, 2000, pp: 62-69

Fiedler, B., Gojny, F.H., "Fundamental aspects of nano-reinforced composites", *Composite Science Technology* 66, 2006, pp: 3115-3125

Fujii, M., Zhang, X., Xie, H., Ago, H., Takahashi, K., Ikuta, T., Abe, H., Shimizu, T., "Measuring the Thermal Conductivity of a Single Carbon Nanotube", *Physical. Review Letters 95*, 2005, 065502 (4pp)

Gao, L., Thostenson, E.T., Zhang, Z., Chou, T.W., "Coupled carbon nanotube network and acoustic emission monitoring for sensing of damage development in composites", *Carbon* 47, 2009, pp: 1381-1388

Gibson, R.F., Ayorinde, E.O., Wen, Y.F., "Vibrations of carbon nanotubes and their composites: a review", *Composite Science Technology 67*, 2007, pp: 1-28

Gojny, F.H., Schulte, K., "Functionalisation effect on the thermo-mechanical behavior of multy-wall carbon nanotube/epoxy-composites", *Composites Science and Technology,* 2004, pp 2303–2308

Gojny, F.H., Wichmann, M.H.G., Fiedler, B., Kinloch, I.A., Bauhofer, W., Windle, A.H., Schulte, K., "Evaluation and identification of electrical and thermal conduction mechanisms in carbon nanotube/epoxy composites*", Polymer 47*, 2006, pp 2036-2045

Heeder, N., Shukla, A., Chalivendra, V., Yang, S., "Sensitivity and dynamic electrical response of CNT-reinforced nanocomposites", *Journal of Material Science 47 Issue 8*, 2011, pp 3808-3816

Heeder, N., Shukla, A., Chalivendra, V., Yang, S., "Electrical response of carbon nanotube reinforced nanocomposites under static and dynamic loading", *Experimental Mechanics 52 Issue 3*, 2011, pp 315-322

Hone, J., Whitney, M.D., Poskoti, C., Zettl, S., "Thermal conductivity of single-walled carbon nanotubes*", Physical Review B 59, number 4*, 1999, pp 2514-2516

Hu, G., Zhao, C., Zhang, S., Yang, M., Wang, Z.. "Low percolation threshold of electrical conductivity and rheology in poly(ethylene terephthalate) through the networks of multi-walled carbon nanotubes", *Polymer* 47, 2006, pp: 480 – 488

Iijima, S., "Helical microtubules of graphitic carbon", *Nature* 354, 1991; pp: 56–58

Kymakis, E., Amaratunga, G.A.J., "Electrical properties of single-wall carbon nano-tube polymer composit films", *Journal of Applied Physics* 99, 2006, 084302

Li, C., Thostenson, E.T., Chou, T.W., "Sensors and actuators based on carbon nanotubes and their composites: A review", *Composites Science and Technology* 68, 2008, pp: 1227-1249

Lim, A.S., An, Q., Chou, T.W., Thostenson, E.T., "Mechanical and electrical response of carbon nanotube-based fabric composites to Hopkinson bar loading", *Composites Science and Technology*, 2011

Moisala, A., Li, Q., Kinloch, I.A., Windle, A.H., "Thermal and electrical conductivity of single- and multi-walled carbon nanotube-epoxy composites", *Composites Science and Technology* 66, 2006, pp 1285-1288

Moniruzzaman, M., Winey, K.I., "Polymer nanocomposites containing carbon nanotubes", *Macromolecules* 39, 2006, pp: 5194-5205

Pham, G.T., Park, Y-B., Wang, B., "Development of carbon nanotube based nanocomposite strain tensor", *ASME Manufacturing Engineering Division* 16-2, 2005, pp: 987-993

Sandler, J.K.W., Kirk, J.E., Kinlock, I.A., Shaffer, M.S.P., Windle, A.H., "Ultra-low electrical percolation threshold in carbon-nanotube-epoxy composites", *Polymer* 44, 2003, pp: 5893–5899

Shenogina, N., Shenogin, S., Xue, L., Keblinski, P., "On the lack of thermal percolation in carbon nanotube composites", *Applied Physics Letters* 87, 2005, pp: 1-3

Song, Y.S., Youn, J.R., "Evaluation of effective thermal conductivity for carbon nanotube/polymer composites using control volume finite element method", *Carbon 44*, 2005, pp 710-717

Thostenson, E.T., Chou, T.W., "Carbon Nanotube Networks: Sensing of Distributed Strain and Damage for Life Prediction and Self Healing", *Advanced Materials* 18, 2006, pp: 2837-2841

Thostenson, E.T., Ren, Z., Chou, T.W., "Advances in the science and technology of carbon nanotubes and their composites: A review", *Composites Science and Technology* 61, 2001, pp: 1899-1912

Vadlamani, V.K., Chalivendra, V., Shukla, A., Yang, S., "In situ sensing of nonlinear deformation and damage in epoxy particulate composites", *Smart Materials and Structures 21*, 2012, 075011 (10pp)

Xie, X.L., Mai, Y.W., Zhou, X.P., "Dispersion and alignment of carbon nanotubes in polymer matrix: a review", *Material Science Engineering* R49, 2005, pp: 89-112